Journal of South American Earth Sciences 58 (2015) 165–187

Contents lists available at ScienceDirect

Journal of South American Earth Sciences

journal homepage: www.elsevier.com/locate/jsames

Paleoproterozoic accretionary and collisional processes and the build-up of the Borborema Province (NE Brazil): Geochronological and geochemical evidence from the Central Domain

Sérgio P. Neves [a, *], Geysson A. Lages [b], Roberta G. Brasilino [b], Alan W.A. Miranda [c]

[a] Departamento de Geologia, Universidade Federal de Pernambuco, 50740-530 Recife, Brazil
[b] CPRM – Serviço Geológico Nacional, Av. Sul 2291, Afogados, Recife, PE 50770-0, Brazil
[c] Universidade Federal Rural do Rio de Janeiro, 21840-600 Rio de Janeiro, Brazil

ARTICLE INFO

Article history:
Received 7 March 2014
Accepted 27 June 2014
Available online 18 July 2014

Keywords:
U–Pb geochronology
Geochemistry
Nd isotopes
Crustal evolution

ABSTRACT

Several Brasiliano-Pan-African belts consist of large areas of reworked Paleoproterozoic rocks. Characterization of these rocks is needed to place better controls on Precambrian paleogeographic reconstructions. The Borborema Province, northeastern Brazil, occupies a central position in West Gondwana configuration, and knowledge of its geological evolution is crucial to infer relationships between Paleoproterozoic units in South America and Africa. Here, we report U–Pb ages, major- and trace-elements analyses and Sm–Nd isotopic data for orthogneisses in the eastern portion of Central Domain. The dominant basement units in the study area are banded gneisses of intermediate composition and relatively juvenile character, and migmatitic gneisses of granitic composition with Archean Nd T_{DM} model ages. One sample of the banded gneiss yielded a weighted $^{207}Pb/^{206}Pb$ age of 2096 ± 23 Ma and an upper intercept age of 2044 ± 27 Ma, which we interpret, respectively, as ages of crystallization and metamorphism. Two large units of migmatitic gneiss in the southern and central parts of the area gave ages of, respectively, 2057 ± 20 Ma and 2055 ± 23 Ma; an orthoamphibolite associated with the latter yielded crystallization age of 2042 ± 11 Ma and metamorphic age of 1996 ± 13 Ma. All these rocks have geochemical signatures typical of subduction zone-related magmas. Combined with evidence provided by previous studies, we suggest that the evolution of the study area starts with island arc construction around 2.2 Ga, leading to an expressive volcanic arc edifice by 2.13–2.10 Ga. By 2.06 Ga, the crust had evolved enough to become intruded by magmas formed at the mantle wedge of the now largely continental magmatic arc, which continued to be intruded by mantle melts until at least 2.04 Ga. An augen gneiss in the northern part of the area, with an age of 2109 ± 15 Ma, and a migmatitic gneiss with a much older age (2183 ± 9 Ma), both of which have geochemical characteristics akin to intraplate magmas, suggest that crustal reworking also took place. The 1981 ± 23 Ma age of a small body of peraluminous felsic gneiss may be related to regional metamorphism and syncollisional magmatism at c. 2.0–1.98 Ga.

1. Introduction

The occurrence and extent of preexisting crust in orogenic belts has important implications for formulation of models of continental growth as well as for paleogeographic reconstructions. In the Gondwana realm, the presence of large fractions of reworked old continental crust in several Pan-African/Brasiliano belts was inferred long ago from reconnaissance geochronological data and/or structural/metamorphic characteristics (e.g., Bertrand and Laserre, 1976; Kroner, 1977; Almeida et al., 1981; Cordani et al., 1999). This assumption is becoming increasingly obvious as the number of precise geochronological data from specific areas accumulates (e.g., Bruguier et al., 1994; Ferré et al., 1996; Toteu et al., 2001; Njiosseu et al., 2005; Dada, 2008). Basement of Paleoproterozoic age in the Borborema Province, northeastern Brazil, was firmly established in the early 1990s (Hackspacher et al., 1990; Van Schmus et al., 1995). In the last decade, there was renewed emphasis on basic geological mapping, which coupled with U–Pb zircon geochronology show that basement orthogneisses are mostly Paleoproterozoic in age (Neves et al., 2004, 2006; Souza

* Corresponding author.
E-mail addresses: serpane36@yahoo.com, serpane@hotlink.com.br (S.P. Neves).

http://dx.doi.org/10.1016/j.jsames.2014.06.009
0895-9811/

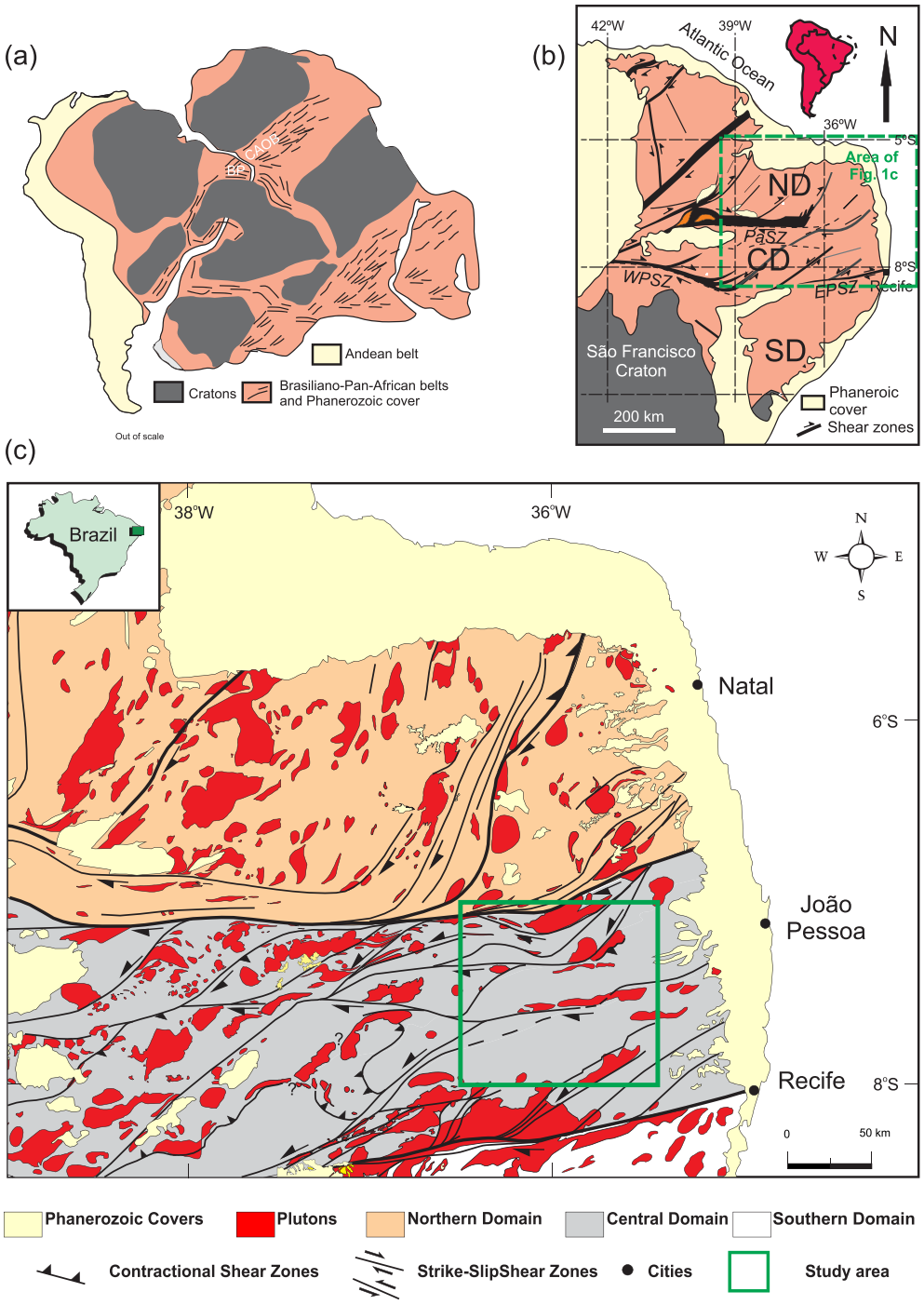

Fig. 1. (a) Pre-drift reconstruction of South America–Africa showing the Andean belt, Archean/Proterozoic cratons and Brasiliano/Pan-African provinces of West Gondwana. BP: Borborema Province; CAOB: Central Africa Orogenic Belt. (b) Sketch showing the subdivision of the Borborema Province in Northern (ND), Central (CD) and Southern (SD) domains. Shear zone systems: PaSZ, Patos; EPSZ, East Pernambuco; WPSZ, West Pernambuco. (c) Simplified geological map (Medeiros et al., 2011) of the area outlined in (b) showing the location of the study area.

et al., 2007; Arthaud et al., 2008; Santos et al., 2008; Van Schmus et al., 2008, 2011; Martins et al., 2009; Hollanda et al., 2011), although small Archean nuclei also exist (Dantas et al., 2004; Arthaud et al., 2008). Furthermore, U–Pb analysis of detrital zircons from metasedimentary sequences show Paleoproterozoic age peaks in several samples (Santos et al., 2004; Neves et al., 2006, 2009; Van Schmus et al., 2003, 2011; Araújo et al., 2012; Guimarães et al., 2012), indicating that Paleoproterozoic rocks were an important, if not dominant, source for the detritus. Finally, the presence of xenocristic zircons in Brasiliano granitoids and Sm–Nd model ages much older than their crystallization ages (Ferreira et al., 1998; Fetter et al., 2000; Mariano et al., 2001; Da Silva Filho et al., 2002; Hollanda et al., 2003; Guimarães et al., 2004; Rodrigues and Brito Neves, 2008; Van Schmus et al., 2008, 2011; Neves et al., 2008) suggest that Paleoproterozoic rocks occur extensively in the deep crust. All these lines of evidence

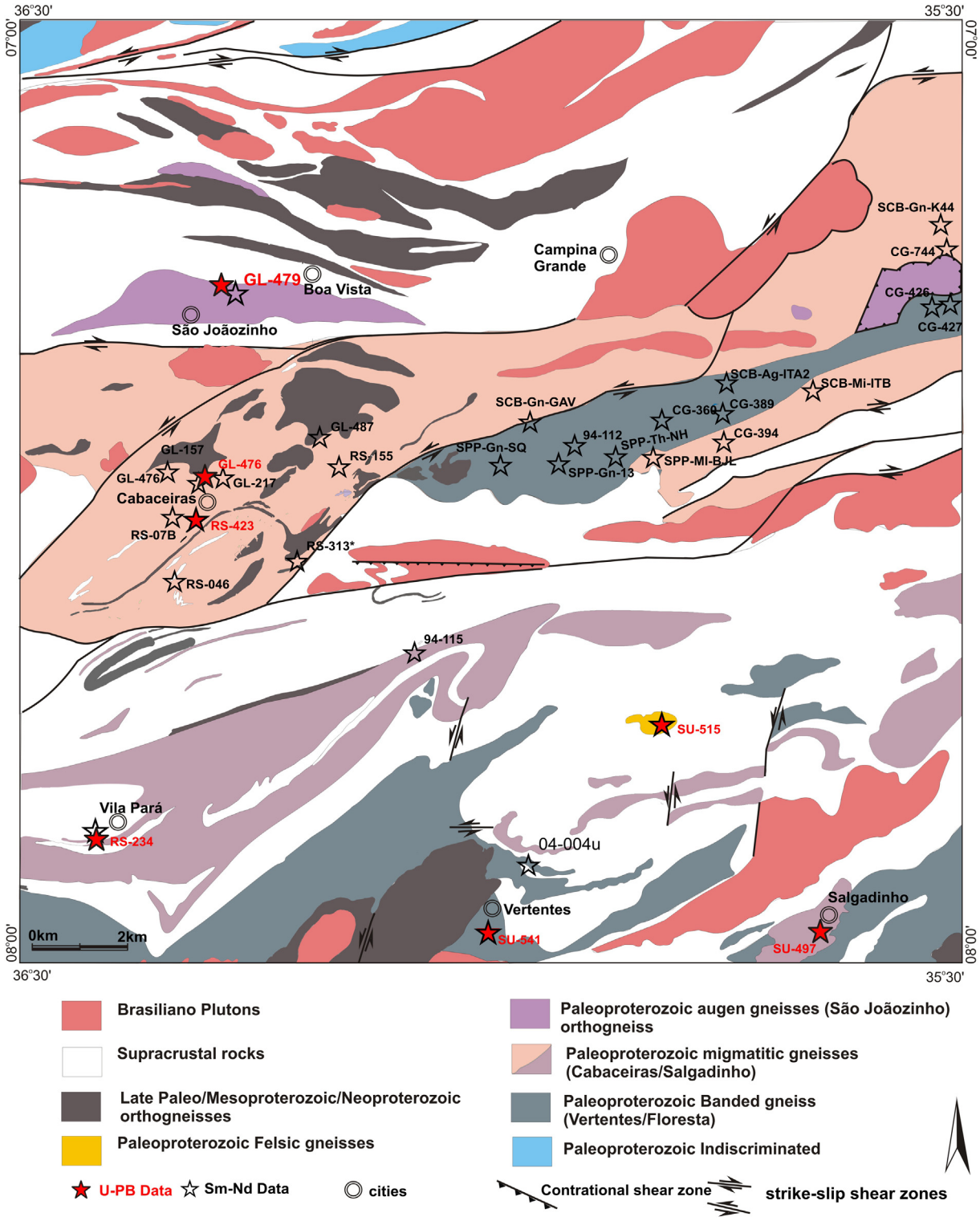

Fig. 2. Geological framework of the study area highlighting main Paleoproterozoic basement rocks and showing the location of U–Pb (LA-ICPMS) and Sm–Nd analyzed samples and from available data. Compiled and modified from Neves et al. (2010), Rodrigues et al. (2010a), Brasilino et al. (2012), Lages and Marinho (2012).

confirm the Paleoproterozoic, particularly the 2.2–2.0 b.y. time span, as the main period of crust formation and/or preservation in the Borborema Province.

The Borborema Province occupies a crucial position in West Gondwana, occurring between the Amazonian, São Luís and São Francisco-Congo cratons and westwards of the Central African Orogenic Belt (Fig. 1a). Therefore, establishing correlations between basement rocks is needed in order to place better controls on paleogeographic reconstructions, not only for the Neoproterozoic but also for the Paleoproterozoic. In this contribution, we present new laser ablation multi-collector inductively coupled-mass spectrometry (LA-MC-ICP-MS) U–Pb zircon ages from orthogneisses in

(a)

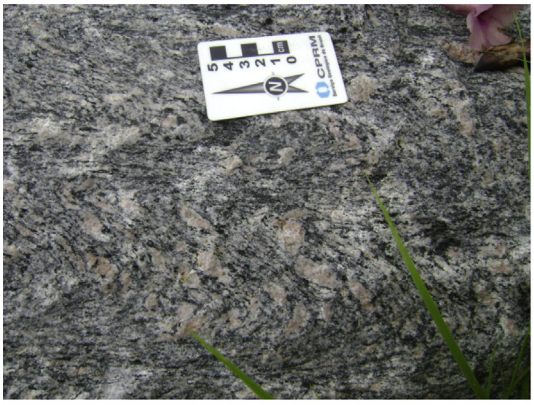

(b)

(c)

(d)

(e)

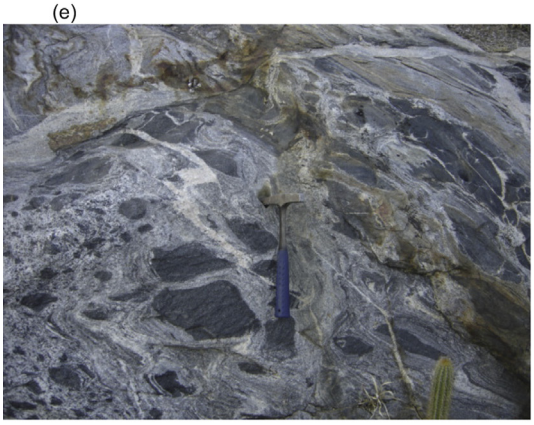

(f)

(g)

(h)

the eastern Borborema Province (Fig. 1b and c). Together with major- and trace elements and Sm–Nd analyses, these data contribute to a better knowledge of the age and nature of Paleoproterozoic events that affected this area. We discuss the role of mantle and crustal sources for the magmatism, the possible environments of intrusion, the number and ages of metamorphic events, and, in conjunction with existing geochronological and geochemical data, propose a tectonic model for the evolution of the study area.

2. Geological setting, petrography and previous U–Pb results

The study area is situated in the eastern portion of the Central Domain, whose limits are the large E-W-striking Patos and Pernambuco transcurrent shear zone systems (Fig. 1c). It comprises an area of about 12 000 km^2 that was mapped at the 1:100 000 scale (Fig. 2). In addition to the orthogneisses subject of this contribution (described below), the study area comprises late Paleoproterozoic to early Mesoproterozoic granitic orthogneisses, metagabbros and meta-anorthosites, small gneissic bodies of early Neoproterozoic age, amphibolite-facies metasedimentary rocks, rare granulitic rocks, and several granitic and syenitic plutons intruded during the Brasiliano orogeny. The orthogneissic basement was extensively reworked during this orogeny. A first deformation phase produced a shallowly to moderately dipping foliation shared by orthogneisses and metasedimentary rocks (Neves et al., 2000, 2005). A second main deformation event gave rise to conjugate sets of dextral, E-W-striking and sinistral, NE-SW-striking subvertical mylonitic belts (Neves and Vauchez, 1995; Neves and Mariano, 1999; Archanjo et al., 2008).

According to their field and petrographic characteristics, the Paleoproterozoic orthogneisses in the study area can be classified into four main groups. The first comprises non-migmatitic and dominantly augen gneisses (Fig. 3a), locally known as São Joãozinho orthogneiss, and is located in the northwestern portion of the area.. It is a biotite-amphibole-bearing gneiss with syenogranitic to monzogranitic composition. The main foliation is defined by stretched quartz that wraps around K-feldspar porphyroclasts. Metamorphism under amphibolite facies conditions is suggested by the association recrystallized K-feldspar + biotite + plagioclase + quartz + titanite. Rodrigues et al. (2010) obtained a U–Pb concordia age of 2137 ± 21 Ma for one sample of augen gneiss whereas two samples dated by Santos et al. (2013) yielded complex results, with $^{207}Pb/^{206}Pb$ ages varying from 2.3 to 1.95 Ga.

The second group of orthogneisses includes migmatized amphibole-biotite-bearing granitic gneisses (Fig. 3b, c, d). They are dominantly coarse-grained (although augen gneisses also occur) and characterized in several outcrops by magnetite-bearing pinkish leucosomes that may be either parallel to or truncate the main foliation. Centimetric to decimetric amphibolitic layers or rounded to elliptic metagabbroic/amphibolitic enclaves occur frequently associated with this group (Fig. 3e). Metagabbroanorthosites, metadiorites, orthoamphibolites (Fig.3f) and massive titanium magnetite ore bodies can also occur locally. In the augen gneisses the fabric is sometimes mylonitic and consists of stretched quartz wrapping around feldspar porphyroclasts. The main mafic phase is amphibole with optical characteristics of hornblende. The paragenesis amphibole + biotite ± (rare)pyroxene + recrystallized plagioclase and K-feldspar + quartz + titanite + opaque minerals reflects amphibolite facies conditions. In some samples, a retrometamorphic assemblage is evidenced by destabilization of pyroxene to amphibole with bluish-green pleochroism that is in turn replaced by epidote, and by replacement of plagioclase by epidote, quartz and calcite. Reaction of hornblende + biotite (first generation) ± plagioclase giving rise to garnet + biotite (second generation) ± microcline suggests maintenance of high temperature conditions during at least two metamorphic events. Assessment of geochemical data (Section 4) demonstrates that these migmatitic orthogneisses belong to three distinct units. We use the terms Salgadinho and Cabaceiras for orthogneissic complexes occurring, respectively, in the southern and central parts of the study area. Santos et al. (2004) obtained an upper intercept age at 2016 ± 27 Ma (MSWD = 0.6) in a biotite-amphibole bearing granitic orthogneiss that we correlated with this group.

The third group of orthogneisses comprises banded gneisses. They dominate in the southern portion of the study area and are referred to as Vertentes Complex around the homologous city and as Floresta Complex elsewhere. These orthogneisses are characterized by regular, centimetric to decimetric, alternating bands with dioritic (dominant) to granitic compositions (Fig. 3g). Fine-grained mafic layers and migmatized portions with concordant and discordant leucosomes may occur locally. Intercalated metamafic rocks (amphibolites and garnet amphibolites), varying from centimetric/decimetric bands to kilometer-long lenses, are a major characteristic of this unit. In the mafic/intermediate bands, the mineralogical assemblage consists of plagioclase, quartz, K-feldspar, biotite, amphibole, garnet and, occasionally, clinopyroxene. Apatite, titanite, allanite and zircon are accessory minerals. Hypidiomorphic prismatic plagioclase crystals with parallel twins and inclusions indicate igneous protolith. Porphyroblastic garnet tends to engulf plagioclase and amphibole from the matrix, indicating metamorphic origin, and may show retrogression to opaque minerals + chlorite. One sample dated by Sá et al. (2002) provided a discordia with upper intercept age of 1970 ± 30 Ma but with a very large MSWD (30). Neves et al. (2006) dated the mafic and felsic portions of a banded sample. In the mafic band they obtained two groups of ages, averaging 2127 ± 7 Ma and 2044 ± 5 Ma. These results were interpreted as ages of crystallization and metamorphism, respectively. One zircon from the felsic band yielded an age of 625 ± 24 Ma, which was inferred as crystallization age and, therefore, the acquisition of the banded structure during the Brasiliano orogeny. A sample of banded gneiss dated by Brito Neves et al. (2013) gave a crystallization age of 2162 ± 7 Ma. In another sample, a few kilometers to the east of the study area, Brito Neves et al. (2013) report crystallization age of 2110 ± 7 Ma, with metamorphic overgrowth at 1983 ± 20 Ma. Analyses of zircons from two samples of granodioritic composition, relatively more homogeneous, defined discordia lines with upper intercepts of 2103 ± 11 Ma (Neves et al., 2006) and 2096 ± 7 Ma (Brito Neves et al., 2013). Lower intercepts of 619 ± 36 Ma and 588 ± 53 Ma, respectively, in these samples confirm Neoproterozoic superimposed metamorphism.

The fourth group of orthogneisses is subordinate in abundance and comprises equigranular felsic granitic gneisses (Fig. 3h) that, in contrast with the previous groups, do not contain amphibole. Sixteen near concordant analyses of zircon grains from one sample dated by Neves et al. (2006) yielded a well-constrained $^{207}Pb/^{206}Pb$

Fig. 3. Field aspects of studied orthogneisses. (a) Non-migmatitic, biotite-amphibole-bearing augen gneiss with syenogranitic to monzogranitic composition (São Joãozinho orthogneiss). (b–d) Migmatized amphibole-biotite-bearing granitic orthogneisses with magnetite-bearing pinkish leucosomes that may be either parallel to or truncate the main foliation (b: Cabaceiras Complex; c: Salgadinho Complex; d: Vila do Pará unit). (e, f) Centimetric amphibolitic layers or rounded to elliptic metagabbroic/amphibolitic enclaves from the Cabaceiras (e) and Salgadinho (f) complexes. In the latter, some mafic enclaves have relatively straight boundaries and may be xenoliths of the Vertentes Complex. (g) Banded gneiss characterized by regular centimetric to decimetric bands of dioritic composition alternating with thin leucocratic bands (Vertentes Complex). (h) Equigranular felsic gneiss.

Table 1
LA-ICPMS U–Th–Pb results for zircons from samples of plutonic rocks of the basement of eastern Borborema Province.

Samples	Th/U	Ratios							ρ	Apparent ages						Conc. (%)
		206 Pb	207 Pb	±1σ	207 Pb	±1σ	206 Pb	±1σ		207 Pb	(Ma)	207 Pb	(Ma)	206 Pb	(Ma)	
Spots		204 Pb	206 Pb		235U		238U			206 Pb		235U		238U		
SU-497 (Salgadinho)																
003-Z01	0.07	178148	0.11595	0.45	3.2984	1.68	0.20632	1.61	0.96	1895	8	1481	13	1209	17.78	81.66
004-Z02	0.20	87087	0.11438	0.50	4.1292	1.93	0.26183	1.86	0.96	1870	9	1660	16	1499	24.85	90.31
016-Z11	0.35	105234	0.13075	0.67	6.0957	1.61	0.33812	1.46	0.91	2108	12	1990	14	1878	23.81	94.37
024-Z16	0.31	205444	0.12680	0.61	6.3123	1.37	0.36106	1.22	0.93	2054	11	2020	12	1987	20.86	98.37
021-Z13	0.24	467687	0.12511	0.67	6.5208	1.73	0.37802	1.60	0.92	2030	12	2049	15	2067	28.28	100.89
006-Z04	0.36	413082	0.12754	0.60	6.6486	1.09	0.37808	0.91	0.89	2064	11	2066	10	2067	16.08	100.07
005-Z03	0.34	397166	0.12790	0.44	6.6630	1.34	0.37784	1.27	0.94	2069	8	2068	12	2066	22.39	99.92
010-Z06	0.33	905425	0.12616	0.49	6.8494	1.08	0.39375	0.97	0.88	2045	9	2092	10	2140	17.60	102.30
027-Z17	0.23	328175	0.12859	0.56	6.8736	1.22	0.38767	1.09	0.88	2079	10	2095	11	2112	19.54	100.80
017-Z12	0.26	132399	0.12911	0.78	6.9536	1.18	0.39062	0.88	0.73	2086	14	2106	10	2126	16.02	100.96
023-Z15	0.17	598069	0.12797	0.44	7.0641	1.05	0.40037	0.95	0.90	2070	8	2120	9	2171	17.51	102.42
011-Z07	0.20	126701	0.12744	0.41	7.0785	1.19	0.40286	1.12	0.94	2063	7	2121	11	2182	20.68	102.87
015-Z09	0.10	1038519	0.12902	0.66	7.1481	1.29	0.40183	1.11	0.85	2085	12	2130	11	2177	20.45	102.23
009-Z05	0.37	546956	0.12667	2.47	7.1968	2.60	0.41205	0.82	0.29	2052	44	2136	23	2224	15.37	104.13
012-Z08	0.27	855232	0.12653	1.01	7.3244	1.21	0.41985	0.67	0.70	2050	18	2152	11	2260	12.72	105.02
030-Z20	0.56	2183059	0.12920	1.87	7.4432	2.47	0.41784	1.62	0.85	2087	33	2166	22	2251	30.68	103.90
029-Z19	0.58	1055276	0.12832	0.98	7.7982	1.70	0.44076	1.39	0.81	2075	17	2208	15	2354	27.40	106.61
022-Z14	0.33	419052	0.13096	0.49	7.8153	1.09	0.43280	0.97	0.88	2111	9	2210	10	2318	18.92	104.90
028-Z18	0.33	526867	0.12806	0.60	7.8227	1.99	0.44303	1.89	0.95	2072	11	2211	18	2364	37.44	106.94
GL-476 (Cabaceiras)																
z01	0.13	95073	0.121497	1.71	5.022	1.31	0.299814	1.10	0.68	1978	30	1823	11	1690	16.41	85.45
z02	0.18	78340	0.121050	0.64	5.047	1.28	0.302399	1.10	0.71	1972	11	1827	11	1703	16.53	86.38
Z03	0.14	48325	0.100339	3.49	2.513	2.59	0.181664	2.34	0.87	1630	63	1276	19	1076	23.16	66.00
z04	0.19	60637	0.119107	1.81	4.560	1.33	0.277694	1.23	0.82	1943	32	1742	11	1580	17.17	81.31
z05	0.22	121456	0.124343	0.47	6.338	1.13	0.369662	1.03	0.81	2019	8	2024	10	2028	17.87	100.41
z06	0.19	15830	0.126051	1.59	5.788	1.21	0.333015	1.03	0.71	2044	28	1945	10	1853	16.56	90.67
Z07	0.13	122288	0.119169	2.97	5.023	2.15	0.305720	2.06	0.92	1944	52	1823	18	1720	30.95	88.47
z08	0.13	115157	0.124472	0.59	6.020	1.13	0.350781	0.97	0.69	2021	10	1979	10	1938	16.17	95.89
z09core	0.09	252976	0.128337	0.81	6.519	1.39	0.368410	1.13	0.61	2075	14	2048	12	2022	19.67	97.43
z10	0.18	47411	0.123179	0.58	5.334	0.98	0.314075	0.79	0.62	2003	10	1874	8	1761	12.19	87.91
z11	0.13	104272	0.123565	1.69	5.740	1.25	0.336928	1.13	0.77	2008	30	1937	11	1872	18.32	93.21
z13	0.11	58659	0.117420	1.87	4.596	1.38	0.283860	1.27	0.80	1917	33	1748	11	1611	18.05	84.01
z14	0.14	75793	0.117193	2.50	4.209	1.87	0.260466	1.66	0.84	1914	44	1676	15	1492	22.02	77.97
z15	0.15	114088	0.123412	1.44	5.740	1.10	0.337329	0.92	0.75	2006	25	1937	9	1874	15.01	93.40
z16	0.13	191156	0.123172	0.53	5.622	1.04	0.331037	0.89	0.76	2003	9	1919	9	1843	14.34	92.05
z17	0.25	63603	0.119684	2.12	4.976	1.56	0.301532	1.44	0.81	1952	37	1815	13	1699	21.47	87.06
z18	0.10	70653	0.119237	2.60	4.847	1.91	0.294792	1.76	0.88	1945	46	1793	16	1665	25.84	85.63
z19	0.32	58475	0.124626	2.01	5.031	1.51	0.292773	1.33	0.81	2023	35	1825	13	1655	19.41	81.81
z20	0.17	64607	0.116724	0.61	3.987	1.48	0.247733	1.35	0.83	1907	11	1632	12	1427	17.25	74.83
z21	0.13	54494	0.121427	0.59	4.743	1.36	0.283302	1.23	0.82	1977	11	1775	11	1608	17.46	81.32
RS-234																
z01	0.03	18134	0.084467	0.91	1.528	1.65	0.131159	1.38	0.67	1303	18	941	10	794	10.31	60.96
z02	0.18	13927	0.130665	0.82	6.313	1.85	0.350420	1.65	0.74	2107	14	2020	16	1937	27.67	91.92
Z03	0.13	16721	0.122891	0.85	4.356	1.93	0.257055	1.73	0.86	1999	15	1704	16	1475	22.78	73.79
Z04	0.14	16151	0.127211	1.29	5.418	3.79	0.308895	3.56	0.92	2060	23	1888	32	1735	54.15	84.24
z05	0.22	27183	0.135319	0.69	7.018	1.47	0.376155	1.29	0.74	2168	12	2114	13	2058	22.79	94.93
z06core	0.17	17595	0.134927	0.68	7.367	1.74	0.395973	1.60	0.79	2163	12	2157	16	2150	29.21	99.42
z07	0.26	25885	0.135052	0.57	7.320	1.19	0.393100	1.05	0.74	2165	10	2151	11	2137	19.13	98.73
Z08	0.00	10511	0.060107	2.39	0.825	3.19	0.099505	2.11	0.66	607	52	611	15	612	12.33	100.67
z09	0.24	34216	0.136604	0.60	7.470	1.59	0.396593	1.47	0.81	2185	11	2169	14	2153	26.96	98.57
z10	0.24	20835	0.136052	0.66	7.647	1.16	0.407654	0.95	0.67	2178	11	2190	10	2204	17.73	101.22
z11	0.20	18295	0.135226	0.76	7.311	1.55	0.392137	1.35	0.71	2167	13	2150	14	2133	24.60	98.42
z13	0.07	20749	0.114581	1.02	3.241	2.16	0.205160	1.91	0.72	1873	18	1467	17	1203	20.96	64.22
z14	0.22	21966	0.136601	0.61	7.233	1.32	0.384043	1.18	0.77	2185	11	2141	12	2095	21.02	95.91
Z15	0.15	44167	0.131900	0.96	5.909	2.05	0.324918	1.81	0.85	2123	17	1963	18	1814	28.65	85.41
z16	0.23	37576	0.136330	0.61	7.331	1.42	0.390023	1.28	0.81	2181	11	2153	13	2123	23.13	97.33
z17	0.23	239834	0.133987	0.65	6.975	1.35	0.377571	1.18	0.77	2151	11	2108	12	2065	20.87	96.00
z18	0.17	27955	0.134083	0.57	7.058	1.33	0.381771	1.20	0.80	2152	10	2119	12	2085	21.38	96.86
Z19	0.17	34123	0.125644	0.97	5.114	1.92	0.295208	1.66	0.84	2038	17	1838	16	1668	24.39	81.83
z20	0.17	24058	0.129251	0.74	5.471	1.52	0.306995	1.33	0.78	2088	13	1896	13	1726	20.15	82.67
z21	0.20	169154	0.135750	0.64	7.126	1.40	0.380706	1.25	0.80	2174	11	2127	12	2080	22.16	95.67
z22	0.17	29712	0.134061	0.72	6.969	1.36	0.377000	1.15	0.73	2152	13	2107	12	2062	20.30	95.84
Z23	0.16	20188	0.134826	1.20	7.180	2.64	0.386256	2.35	0.87	2162	21	2134	24	2105	42.26	97.39
z24	0.20	48806	0.133861	0.61	6.586	1.26	0.356814	1.10	0.76	2149	11	2057	11	1967	18.70	91.52
z25	0.17	31060	0.129885	0.62	5.456	1.23	0.304667	1.06	0.75	2096	11	1894	11	1714	15.92	81.78
z26	0.02	9972	0.091555	1.11	1.766	1.89	0.139904	1.53	0.64	1458	21	1033	12	844	12.10	57.89
z27	0.27	42787	0.135533	0.68	7.062	1.42	0.377902	1.25	0.80	2171	12	2119	13	2066	22.07	95.19
RS-423 (orthoamphibolite)																
larger zircons																
z04	0.44	10016	0.125843	1.04	6.405	4.00	0.369114	3.86	0.97	2041	18	2033	35	2025	67	99.24
z06	0.49	99569	0.126777	0.57	6.320	1.23	0.361540	1.09	0.88	2054	10	2021	11	1989	19	96.87

Table 1 (*continued*)

Samples	Th/U	Ratios							ρ	Apparent ages						Conc. (%)
		206 Pb	207 Pb	±1σ	207 Pb	±1σ	206 Pb	±1σ		207 Pb	(Ma)	207 Pb	(Ma)	206 Pb	(Ma)	
Spots		204 Pb	206 Pb		235U		238U			206 Pb		235U		238U		
z07	0.44	6229	0.126679	1.05	6.509	3.95	0.372627	3.81	0.96	2052	19	2047	35	2042	67	99.48
Z08	0.43	18393	0.125677	0.83	6.450	2.18	0.372214	2.01	0.92	2038	15	2039	19	2040	35	100.07
z09	0.30	17032	0.124685	0.74	6.319	1.86	0.367588	1.71	0.91	2024	13	2021	16	2018	30	99.69
z10	0.36	25808	0.125905	0.92	6.158	1.80	0.354743	1.54	0.93	2042	16	1999	16	1957	26	95.87
z01	0.31	4565	0.124898	1.45	5.897	6.21	0.342419	6.02	0.97	2027	25	1961	53	1898	99	93.63
Z02	0.23	2135	0.128024	1.58	6.048	4.76	0.342639	4.47	0.94	2071	28	1983	41	1899	73	91.71
small zircons																
Z11	0.09	10495	0.123309	0.85	5.736	2.67	0.337345	2.52	0.95	2005	15	1937	23	1874	41	93.48
Z14	0.14	14536	0.123150	0.84	5.684	2.13	0.334766	1.95	0.92	2002	15	1929	18	1861	32	92.96
z16	0.10	12335	0.122028	0.80	6.112	3.40	0.363238	3.30	0.97	1986	14	1992	29	1998	57	100.58
Z18	0.06	14086	0.121585	0.82	5.697	2.65	0.339842	2.51	0.95	1980	15	1931	23	1886	41	95.27
z19	0.08	5497	0.123663	0.87	5.217	3.24	0.305984	3.11	0.96	2010	15	1855	27	1721	47	85.63
z12	0.04	5043	0.134641	1.10	7.554	5.03	0.406917	4.91	0.98	2159	19	2179	45	2201	92	101.92
z13	0.09	3490	0.127969	3.40	5.877	12.38	0.333097	11.85	0.99	2070	59	1958	102	1853	189	89.52
Z15	0.04	4217	0.127501	1.56	6.675	6.17	0.379707	5.94	0.97	2064	27	2069	53	2075	105	100.54
Z17	0.18	4591	0.161203	1.45	8.863	8.64	0.398749	8.49	0.99	2468	24	2324	76	2163	155	87.64
GL-479 (São Joãozinho)																
z01	0.13	50617	0.121702	0.97	4.638	1.40	0.276404	1.02	0.68	1981	17	1756	12	1573	14.18	79.40
z02core	0.14	44173	0.125627	0.87	5.470	1.37	0.315764	1.07	0.69	2038	15	1896	12	1769	16.51	86.82
z03	0.13	12385	0.131039	0.98	7.504	2.40	0.415314	2.20	0.79	2112	17	2173	22	2239	41.55	106.02
z04	0.14	74015	0.129503	0.69	6.447	1.24	0.361042	1.03	0.72	2091	12	2039	11	1987	17.62	95.02
z05core	0.17	41453	0.128952	0.65	6.196	1.24	0.348501	1.05	0.73	2084	11	2004	11	1927	17.53	92.50
z06	0.24	40705	0.130336	1.06	6.818	1.59	0.379406	1.19	0.71	2102	19	2088	14	2074	21.15	98.62
z07	0.14	16301	0.129984	0.85	6.583	1.73	0.367291	1.51	0.72	2098	15	2057	15	2017	26.10	96.13
z08	0.31	23807	0.130951	0.77	6.864	1.64	0.380177	1.45	0.73	2111	14	2094	15	2077	25.72	98.41
z09	0.18	16680	0.127232	0.68	5.627	1.72	0.320775	1.58	0.80	2060	12	1920	15	1794	24.76	87.06
z10	0.23	8248	0.127089	1.71	5.737	2.84	0.327422	2.27	0.80	2058	30	1937	25	1826	36.13	88.72
z11	0.10	15709	0.130906	0.83	6.581	1.89	0.364625	1.69	0.78	2110	14	2057	17	2004	29.19	94.97
z12	0.14	39018	0.121411	0.85	5.151	1.81	0.307685	1.60	0.75	1977	15	1845	15	1729	24.22	87.47
z13	0.25	37516	0.131081	0.60	6.860	1.34	0.379545	1.20	0.80	2112	11	2093	12	2074	21.27	98.19
z14	0.32	18532	0.128757	1.00	6.216	1.96	0.350155	1.69	0.73	2081	18	2007	17	1935	28.22	93.00
z15	0.29	12685	0.129475	1.00	6.901	2.38	0.386579	2.16	0.78	2091	18	2099	21	2107	38.91	100.77
z16rim	0.10	16344	0.128660	1.50	6.402	2.23	0.360859	1.65	0.72	2080	26	2032	20	1986	28.22	95.50
z16core	0.17	23628	0.123737	0.88	5.636	2.19	0.330344	2.00	0.80	2011	16	1922	19	1840	32.07	91.51
z17	0.27	128880	0.121907	1.08	4.708	1.78	0.280092	1.42	0.70	1984	19	1769	15	1592	20.00	80.22
z18	0.23	22712	0.129436	0.94	7.014	2.09	0.392987	1.87	0.78	2090	17	2113	19	2137	33.96	102.22
z19	0.15	12669	0.129679	0.94	7.024	2.05	0.392828	1.82	0.77	2094	17	2114	18	2136	33.09	102.02
z20	0.16	18897	0.125094	1.32	5.673	1.86	0.328884	1.31	0.71	2030	23	1927	16	1833	20.87	90.29
SU-541 (Vertentes)																
003-Z01	0.22	1255508	0.12136	0.90	5.9510	1.70	0.35565	1.44	0.84	1976	16	1969	15	1962	24.38	99.25
004-Z02	0.18	1200	0.13846	1.45	7.4169	1.90	0.38849	1.22	0.63	2208	25	2163	17	2116	22.00	95.82
005-Z03	0.41	3867	0.14059	0.72	8.2573	1.29	0.42596	1.07	0.82	2235	12	2260	12	2287	20.55	102.37
006-Z04	0.12	538398	0.12664	0.60	6.9037	1.07	0.39538	0.88	0.86	2052	11	2099	9	2148	16.12	104.67
009-Z05	0.40	325069	0.12952	0.54	7.3045	1.15	0.40903	1.01	0.87	2091	10	2149	10	2211	18.90	105.69
010-Z06	0.32	2654	0.13821	0.86	6.6659	1.71	0.34980	1.47	0.86	2205	15	2068	15	1934	24.68	87.70
011-Z07	0.17	96580	0.12355	0.48	6.3203	1.54	0.37101	1.47	0.95	2008	9	2021	14	2034	25.56	101.30
012-Z08	0.39	466014	0.12633	0.82	7.3708	1.34	0.42315	1.07	0.88	2048	14	2157	12	2275	20.42	111.09
015-Z09	0.21	32911	0.12690	0.62	5.7724	2.82	0.32990	2.75	0.98	2056	11	1942	24	1838	43.80	89.41
016-Z10	0.19	32312	0.12717	0.50	6.1263	1.23	0.34940	1.12	0.91	2059	9	1994	11	1932	18.74	93.81
017-Z11	0.22	220748	0.12359	0.50	5.3877	0.94	0.31617	0.79	0.82	2009	9	1883	8	1771	12.25	88.17
018-Z12	0.59	45590	0.12310	0.50	6.4119	1.44	0.37777	1.35	0.96	2002	9	2034	13	2066	23.84	103.21
021-Z13	0.31	197888	0.12622	1.80	5.6470	2.36	0.32448	1.53	0.64	2046	31	1923	20	1812	24.14	88.54
022-Z14	0.24	95112	0.12771	0.44	7.2659	1.00	0.41263	0.90	0.89	2067	8	2145	9	2227	16.96	107.75
023-Z15	0.10	1450340	0.12770	0.47	7.1922	1.60	0.40847	1.53	0.95	2067	8	2136	14	2208	28.64	106.84
027-Z16	0.29	1566940	0.12680	0.64	5.8995	1.35	0.33743	1.19	0.87	2054	11	1961	12	1874	19.31	91.25
028-Z17	0.15	408838	0.12017	1.91	6.0963	2.35	0.36793	1.36	0.57	1959	34	1990	20	2020	23.58	103.11
029-Z18	0.06	319407	0.11986	0.91	5.6091	1.78	0.33941	1.53	0.85	1954	16	1918	15	1884	24.94	96.40
030-z19	0.24	374102	0.13487	7.61	7.9474	11.18	0.42737	8.19	0.91	2162	133	2225	101	2294	157.99	106.08
033-Z20	0.12	3790	0.14488	1.47	6.9861	1.81	0.34972	1.04	0.56	2286	25	2110	16	1933	17.46	84.56
034-Z21	0.21	60268	0.12945	0.46	7.4638	1.79	0.41818	1.72	0.96	2090	8	2169	16	2252	32.77	107.74
035-Z22	0.60	298764	0.12779	0.49	6.9507	1.38	0.39449	1.29	0.93	2068	9	2105	12	2144	23.59	103.67
036-z23	0.22	246934	0.12036	0.71	6.4773	1.33	0.39033	1.13	0.92	1962	13	2043	12	2124	20.40	108.30
039-Z24	0.08	211025	0.12366	0.65	6.5183	1.27	0.38230	1.09	0.85	2010	12	2048	11	2087	19.47	103.84
040-Z25	0.32	258598	0.13028	0.47	7.3547	1.01	0.40942	0.90	0.87	2102	8	2155	9	2212	16.78	105.26
041-Z26	0.42	443388	0.13134	0.54	7.3288	1.47	0.40469	1.37	0.93	2116	9	2152	13	2191	25.41	103.52
042-z27	0.28	6657	0.12898	1.88	6.7247	2.25	0.37814	1.23	0.77	2084	33	2076	20	2068	21.74	99.21
SU-515 (felsic gneiss)																
047-Z30	0.07	212	0.07016	26.72	0.7880	27.07	0.08146	4.36	0.31	933	548	590	121	505	21.18	54.11
018 Z12	0.07	41174	0.10937	1.73	5.670476	2.40	0.37602	1.67	0.72	1789	31	1927	21	2058	29.34	115.02
025 Z16	0.09	250	0.09282	5.04	1.629833	5.34	0.12735	1.76	0.33	1484	95	982	34	773	12.81	52.06
056-Z35	0.09	1971	0.12964	1.34	6.9918	1.67	0.39117	0.99	0.57	2093	24	2110	15	2128	17.98	101.68

(*continued on next page*)

Table 1 (*continued*)

Samples	Th/U	Ratios							ρ	Apparent ages						Conc. (%)
		206 Pb	207 Pb	±1σ	207 Pb	±1σ	206 Pb	±1σ		207 Pb	(Ma)	207 Pb	(Ma)	206 Pb	(Ma)	
Spots		204 Pb	206 Pb		235U		238U			206 Pb		235U		238U		
019 Z13	0.09	133867	0.10899	1.49	5.193905	3.05	0.34563	2.66	0.87	1783	27	1852	26	1914	44.08	107.35
058-Z37	0.12	2258	0.11440	2.15	5.9778	2.44	0.37899	1.17	0.46	1870	39	1973	21	2072	20.67	110.76
036 Z25	0.12	42311	0.11527	1.12	5.873405	2.08	0.36956	1.76	0.84	1884	20	1957	18	2027	30.57	107.61
045-Z28	0.12	59	0.13273	1.29	5.9634	6.30	0.32586	4.65	0.96	2134	22	1971	53	1818	96.97	85.19
030 Z21	0.16	21496	0.12486	1.07	6.805503	2.03	0.39531	1.72	0.85	2027	19	2086	18	2147	31.45	105.95
031 Z22	0.16	61078	0.11792	1.26	5.789927	2.19	0.35610	1.79	0.81	1925	22	1945	19	1964	30.32	102.01
015 Z09	0.18	30452	0.11822	1.72	6.668465	2.22	0.40911	1.40	0.62	1929	31	2068	20	2211	26.17	114.58
053-Z34	0.18	506766	0.12151	2.10	6.6542	2.26	0.39719	0.83	0.58	1978	37	2067	20	2156	15.24	108.98
029 Z20	0.19	10001	0.12150	1.87	6.148167	3.17	0.36700	2.57	0.81	1978	33	1997	28	2015	44.42	101.87
035 Z24	0.22	95374	0.11275	1.02	6.987447	1.63	0.44945	1.28	0.77	1844	18	2110	15	2393	25.49	129.74
046-Z29	0.25	250	0.13438	1.12	7.2590	1.52	0.39177	0.96	0.63	2156	19	2144	13	2131	18.52	98.84
032 Z23	0.26	11007	0.13060	1.94	6.985509	3.22	0.38793	2.57	0.84	2106	34	2110	28	2113	46.22	100.34
004 Z02	0.26	16004	0.12237	1.06	6.568921	1.96	0.38934	1.64	0.84	1991	19	2055	17	2120	29.65	106.46
026 Z17	0.28	6252	0.12258	3.13	6.278343	4.20	0.37147	2.78	0.66	1994	55	2015	36	2036	48.72	102.12
009 Z05	0.30	25671	0.09598	1.20	2.370679	2.60	0.17914	2.30	0.88	1547	22	1234	18	1062	22.54	68.65
020 Z14	0.31	23650	0.10750	2.08	2.83201	3.58	0.19106	2.91	0.81	1758	38	1364	27	1127	30.04	64.13
012 Z08	0.31	15868	0.11332	3.13	6.439738	3.99	0.41217	2.47	0.75	1853	57	2038	35	2225	46.56	120.05
028 Z19	0.32	10693	0.11108	2.55	3.636655	3.32	0.23744	2.12	0.75	1817	46	1558	26	1373	26.20	75.57
003 Z01	0.33	17919	0.11037	1.61	3.854067	5.00	0.25327	4.73	0.95	1805	29	1604	40	1455	61.40	80.61
0317Z26	0.33	8624	0.11465	1.43	3.76107	2.38	0.23792	1.91	0.80	1874	26	1584	19	1376	23.61	73.40
044-Z27	0.37	18596	0.11264	0.93	3.6615	1.66	0.23576	1.38	0.82	1842	17	1563	13	1365	16.94	74.06
059-Z38	0.38	152598	0.11541	1.63	4.2015	2.93	0.26404	2.44	0.94	1886	29	1674	24	1510	32.71	80.08
005 Z03	0.38	22165	0.12039	1.32	6.10018	2.50	0.36748	2.12	0.85	1962	24	1990	22	2018	36.78	102.83
006 Z04	0.42	16954	0.10433	8.91	5.629647	9.64	0.39135	3.68	0.62	1703	164	1921	83	2129	66.80	125.05
016 Z10	0.43	27751	0.11571	1.79	5.528955	2.45	0.34655	1.68	0.68	1891	32	1905	21	1918	27.81	101.43
027 Z18	0.44	11528	0.11816	1.37	5.370307	2.51	0.32963	2.10	0.84	1929	24	1880	21	1837	33.59	95.23
057-Z36	0.44	3687	0.12897	1.43	6.2149	3.71	0.34948	3.41	0.92	2084	25	2007	32	1932	56.85	92.71
010 Z06	0.47	8534	0.07261	9.34	3.28981	9.49	0.32859	1.71	0.18	1003	190	1479	74	1832	27.28	182.58
051-Z32	0.53	2506	0.10103	1.15	3.3320	1.83	0.23920	1.41	0.77	1643	21	1489	14	1383	17.67	84.14
011 Z07	0.56	431	0.09392	5.12	3.250166	8.51	0.25098	6.55	0.79	1507	94	1469	64	1444	87.36	95.82
050-Z31	0.63	150	0.05942	7.97	1.0462	9.82	0.12769	5.08	0.54	583	164	727	50	775	41.75	132.96
017 Z11	0.65	11809	0.11459	1.83	6.185003	2.79	0.39147	2.11	0.75	1873	33	2002	24	2130	38.20	113.67
052-Z33	0.85	85	0.11046	1.83	1.5926	4.68	0.10457	3.42	0.88	1807	33	967	29	641	26.20	35.48

weighted mean age of 1991 ± 5 Ma, which suggests that this magmatism is the youngest in the studied area.

3. U–Pb geochronology and Nd isotopes

3.1. Methods

Zircons were separated using conventional techniques. After crushing and sieving of the powdered samples, heavy minerals were concentrated by panning and then by heavy liquids. The heavy mineral concentrates were subsequently processed by magnetic separation on a Frantz separator. The grains were then mounted on adhesive tape and enclosed in epoxy resin. After 1–2 days of drying, the mounts were removed from the tape and polished to about half of their thickness. U–Pb zircon ages were obtained at the *Universidade de Brasília*, Brazil, using a Thermo Finningan Neptune multi-collector ICP-MS attached to a New Wave 213 μm Nd-YAG solid state laser. Analytical procedures are detailed by Buhn et al. (2009). Ages were calculated using the Isoplot program of Ludwig (2000) and quoted with 95% confidence intervals. Errors for single analysis and mean ages are quoted, respectively, at the 1σ and 2σ levels.

Sm–Nd analysis followed the method described by Gióia and Pimentel (2000). Whole-rock powders (ca. 50 mg) and leached minerals were mixed with ^{149}Sm–^{150}Nd spike solution and dissolved in savillex capsules. Sm and Nd extraction of whole-rock samples followed conventional cation exchange techniques, using Teflon columns containing LN-Spec resin (HDEHP – diethylhexil phosphoric acid supported on PTFE powder). Sm and Nd samples were loaded on Re evaporation of double filament assemblies and the isotopic measurements were carried out on a multi-collector Finnigan MAT 262 mass spectrometer in static mode.

Uncertainties of Sm/Nd and ^{143}Nd/^{144}Nd ratios are better than ±0.4% (1 σ) and ±0.005% (1 σ) respectively, based on repeated analyses of international rock standards BHVO-1 and BCR-1. ^{143}Nd/^{144}Nd ratios were normalized to ^{146}Nd/^{144}Nd of 0.7219 and the decay constant used was 6.54×10^{-12}. T_{DM} model ages values were calculated using the DePaolo (1981) model.

3.2. Dated Samples

Seven samples were chosen for this study. Three (SU-497, RS-234 and GL-476) are from the mesosome of migmatitic orthogneisses. SU-497 was collected in the type area of the Salgadinho Complex (35°45'25"W, 7°43'25"S; Fig. 3b), RS-234 in a quarry near Vila Pará Village, Santa Cruz do Capibaribe town (36°22'06"W, 7°50'47"S; Fig. 3d), and GL-476 in the Cabaceiras quarry, around Cabaceiras city (36°18'11"W, 7°28'59"S; Fig. 3c). The fourth sample (RS-423) is from a dark green, fine- to medium-grained, granoblastic orthoamphibolite associated with granitic gneisses of the Cabaceiras unit in the northern part of the area (36°18'45"W, 7°31'43"S; Fig. 3e). Sample GL-479 is from an augen gneiss in the type area of São Joãozinho orthogneiss, around São Joãozinho village (36°16'30"W, 7°17'01"S; Fig. 3a). Sample SU-541 is from the mafic band of a banded orthogneiss and was collected at Pedreira do Tito, c. 1.5 km north of the type locality of the Vertentes Complex (35°53'46"W, 7°42'15"S; Fig. 3f). The last sample (SU-515) is from an equigranular felsic gneiss sampled at coordinates 35°48'38"W, 7°44'39"S. The data obtained in this study are presented in Table 1 and plotted in Concordia diagrams on Figs. 4 and 5.

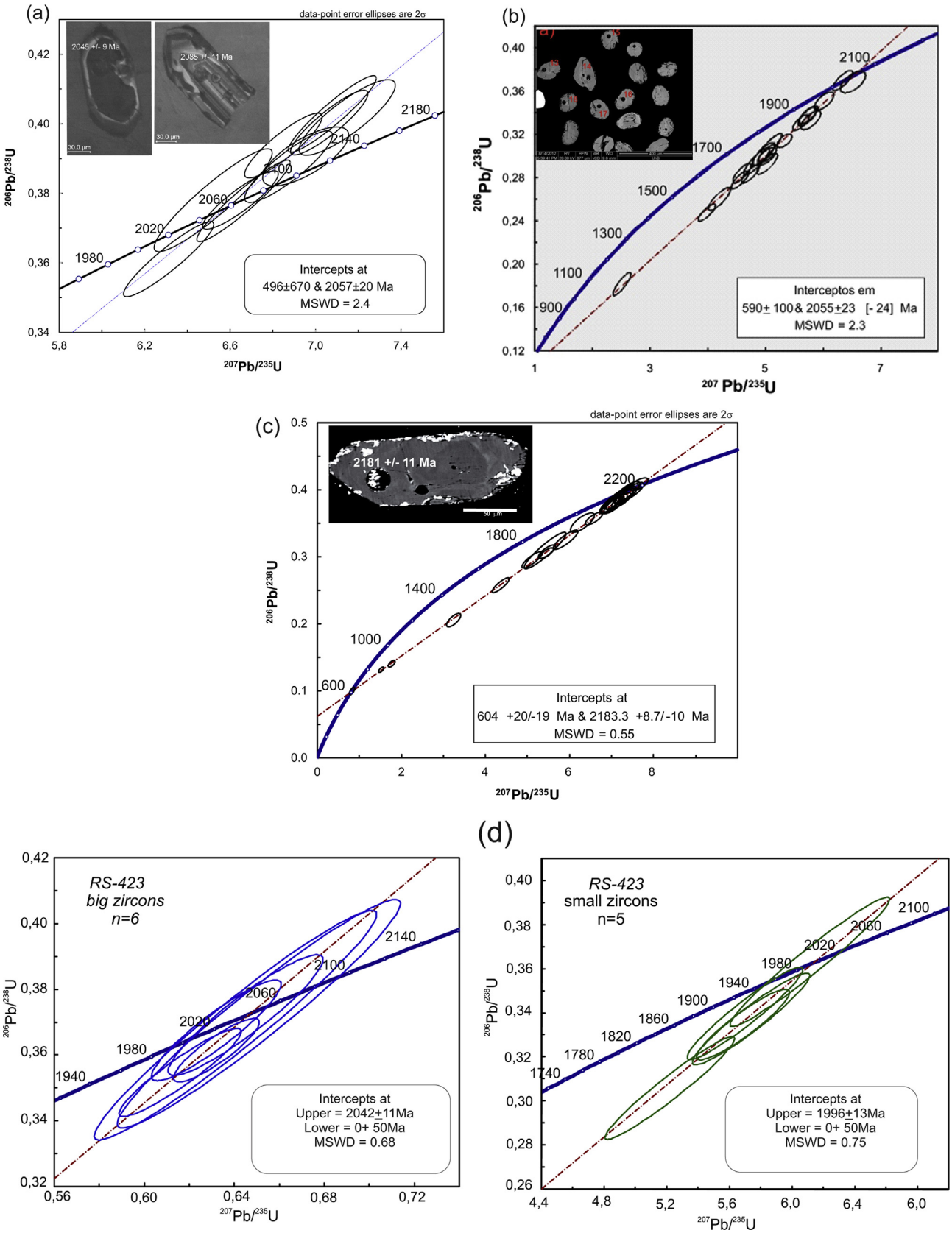

Fig. 4. U–Pb concordia diagrams and representative images of the analyzed zircon grains. (a) SU-497 (Salgadinho Complex). (b) GL-476 (Cabaceiras Complex). (c) RS-234. (d) RS-423 (orthoamphibolite). Left: large zircon grains; right: smaller zircon grains.

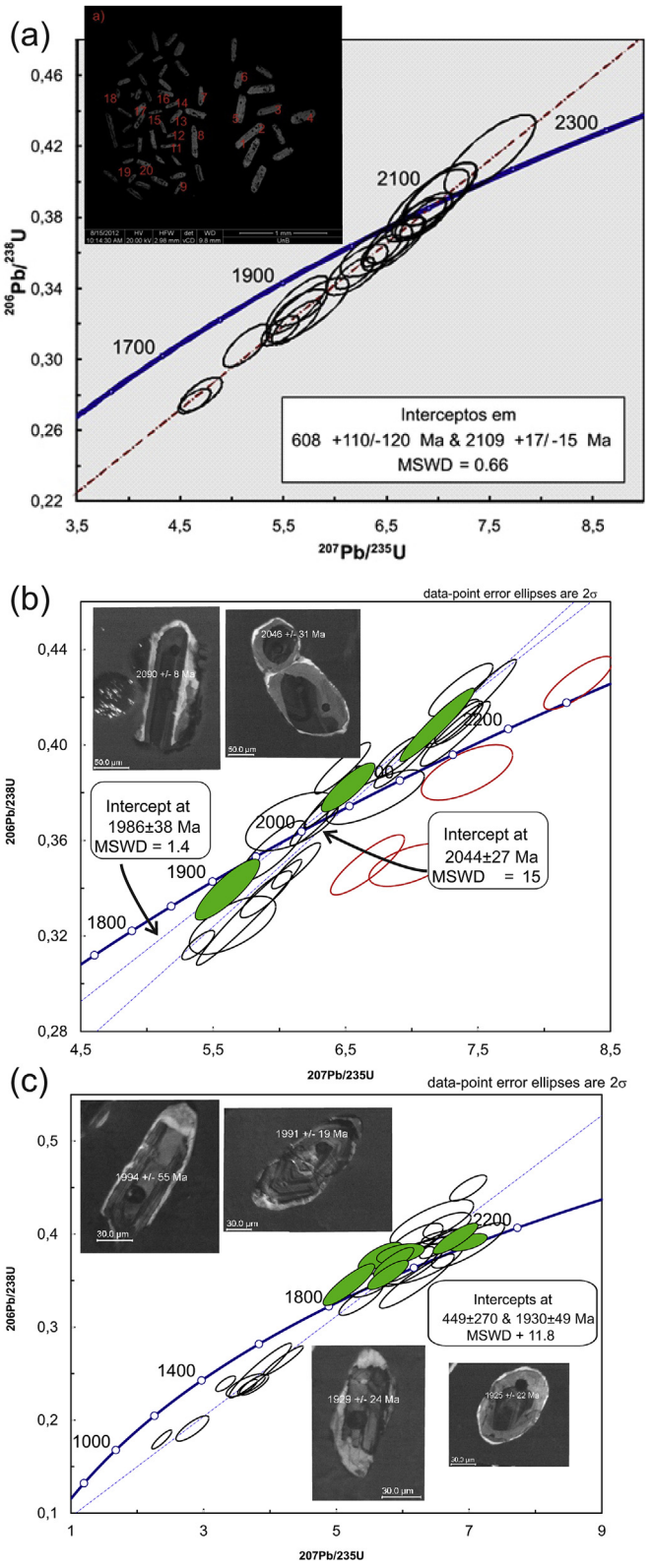

Fig. 5. U–Pb concordia diagrams and representative images of the analyzed zircon grains. (a) GL-479 (São Joãozinho orthogneiss). (b) SU-541 (Vertentes Complex). Inset shows catholuminescence images of a euedral zircon with oscillatory zoning (left) and a core of oscillatory zoned zircon with an embayed morphology (right). (c) SU-515 (felsic gneiss). Green elipses in (b) and (c) are analyses from zircon crystals with Th/U < 0.1; red elipses are analyses not used in age calculations. (For interpretation of the references to colour in this figure legend, the reader is referred to the web version of this article.)

3.3. U–Pb results

3.3.1. Migmatitic orthogneisses

3.3.1.1. Sample SU-497 (Salgadinho Complex). Nineteen analyses were performed on 19 grains. The grains are subhedral to euhedral, show oscillatory zoning and have overgrowth rims of variable width (Fig. 4a). The analyses yielded a discordia with upper intercept at 2057 ± 20 Ma (MSWD = 2.4), which is taken as our best estimate for emplacement of the protolith. This age is similar within error to the $^{207}Pb/^{206}Pb$ weighted mean age of 2065 ± 13 Ma obtained in a cluster of ten concordant analyses (Fig. 4a).

3.3.1.2. Sample GL-476 (Cabaceiras unit). Twenty one analyses were obtained from 21 zircon grains. The grains have rounded morphologies and most present internal fractures (Fig. 4b). Regression of all data gave a discordia with upper intercept at 2055 ± 23 Ma (MSWD = 2.3; Fig. 4b), which is considered to represent the crystallization age of the protolith. This age is similar to that found in sample SU-497. A core spot (#z09) with Th/U ratio lower than 0.1 yielded a $^{207}Pb/^{206}Pb$ value of 2075 ± 14 Ma. It is possible that this grain is a xenocryst formed in a previous metamorphic event.

3.3.1.3. Sample RS-234. Twenty six analyses were performed on 26 six grains. They define a discordia line with upper intercept at 2183 ± 9 Ma and lower intercept at 604 ± 20 Ma (MSWD = 0.55; Fig. 4c). Twelve analyses that plot close to concordia yielded a $^{207}Pb/^{206}Pb$ weighted average age of 2170 ± 70 Ma (MSWD = 0.007), which is in accordance with the upper intercept age. These results indicate that the crystallization age of this orthogneiss is considerably older than that of samples SU-497 and GL-476. Despite the field and petrographic resemblance of this sample to other migmatitic orthogneisses, it differs on geochemical grounds (see Section 4). The lower intercept age corresponds to metamorphism related to the Brasiliano-Pan African event and is constrained by analysis Z08 (Table 1), which yielded a $^{206}Pb/^{238}U$ age of 612 ± 12 Ma and has Th/U ratio less than detection limit (0.00).

3.3.2. Orthoamphibolite (RS-423)

Eleven analyses were accomplished on 11 zircon crystals of sample RS-423. Two groups of zircons with different discordia ages were identified (Fig. 4d). The first group is formed by larger zircons with oscillatory zoning. Six analyses (Z04, Z06, Z07, Z08, Z09, Z10) that plot close to concordia yielded a discordia with upper intercept at 2042 ± 11 Ma. This age is interpreted as the crystallization age of the protolith in view of the elevated Th/U ratios (>0.3) coupled with low MSWD (0.68). The other group is characterized by smaller elongated zircons with faces well preserved. Five discordant analyses (Z11, Z14, Z16, Z18, Z19) define a discordia with upper intercept at 1996 ± 13 Ma. Th/U ratios lower than 0.1 obtained from four analyses of this group (#Z11,#Z16, #Z18, #Z19) suggest a metamorphic origin.

3.3.3. São Joaozinho augen gneiss (GL-479)

Zircon grains from sample GL-479 are yellowish to colourless, and present well preserved prismatic habit and faces (Fig. 5a). Twenty one analyses were obtained from 20 grains. The weighted mean $^{207}Pb/^{206}Pb$ age of 2100 ± 9.7 Ma obtained in a cluster of nine concordant analyses (less than 5% discordance) and with Th/U ratios greater than 0.1 is taken as the best estimate for the age of crystallization of the protolith. This age is similar to the upper intercept age of 2109 ± 15 Ma (MSWD = 0.66) obtained by regression of all data.

Table 2
Summary of new and available Sm–Nd data from rocks related to the Paleoproterozoic basement in eastern Borborema. References: 1. Rodrigues and Brito Neves (2008); 2. Brito Neves et al. (2001b); 3. Brito Neves et al. (2001a); 4. Dantas, 1997; 5. Van Schmus et al. (2011); 6. This paper.

Sample	S lat	W long	Nd (ppm)	Sm (ppm)	$^{147}Sm/^{144}Nd$	$^{143}Nd/^{144}Nd$	eNd (now)	eNd (2050)	T_{DM} (Ga)	
Cabaceiras Complex										
GL-157	7.464	36.342	7.601	1.921	0.1528	0.511751	−17.31	−5.82	3.28	6
GL-217	7.484	36.284	38.113	7.9453	0.126	0.51129	−26.29	−7.81	3.06	6
GL-476	7.483	36.303	16.343	2.304	0.0852	0.510729	−37.25	−8.08	2.74	6
GL-487	7.179	36.050	49.883	9.198	0.1115	0.510895	−33.99	−11.72	3.22	6
RS-046	7.594	36.335	31.581	7.78	0.0915	0.510706	−37.68	−10.18	2.92	6
RS-07B	7.524	36.336	1.911	0.906	0.2865	0.512598	−0.78	−24.26		6
CG-744	7.242	35.517	34.408	5.618	0.09874	0.51113	−29.34	−3.80	2.55	
CG-394	7.446	35.753	15.267	4.255	0.16854	0.51214	−9.64	−2.35	3.12	
SCB-Mi-ITB	7.392	35.658	18.93	3.11	0.09976	0.51096	−32.73	−7.38	2.81	
SPP-MI-BJL	7.463	35.828			0.1171	0.51102	−31.56	−10.75	3.25	
SCB-Gn-K44	7.215	35.523	18.46	3.8	0.12436	0.51141	−23.9	−5.04	2.81	4
Salgadinho Complex										
RS-155	7.472	36.160	25.05	3.195	0.0771	0.51066	−38.59	−7.31	2.65	6
RS-313	7.573	36.205	281.565	40.904	0.0878	0.510872	−34.45	−5.97	2.62	6
São Joãozinho Orthogneiss										
GL-479	7.284	36.275	55.921	10.514	0.1136	0.511059	−30.81	−9.07	3.03	6
Vertentes/Floresta Complex										
04-004u	7.895	35.96	25.07	4.46	0.1076	0.511361	−24.9	−1.61	2.43	
CG-360	7.423	35.819	18.228	3.103	0.10294	0.51118	−28.4	−3.92	2.58	
CG-389	7.416	35.754	2.412	0.421	0.10565	0.51145	−23.2	0.63	2.26	
CG-426	7.300	35.513	19.787	9.772	0.29862	0.51204	−11.64	−38.32		
CG-427	7.300	35.496	21.273	4.717	0.13408	0.51168	−18.67	−2.31	2.63	
94–115	7.67	36.081	17.61	3.01	0.10352	0.511441	−23.4	1.02	2.22	
SPP-Gn-13	7.469	35.928	29.326	6.035	0.1247	0.51162	−19.96	−1.03	2.46	
SPP-Th-NH	7.450	35.910	6.692	1.194	0.1079	0.51141	−24.05	−0.73	2.37	
SPP-Gn-SQ	7.450	35.910	4.91	0.86	0.10649	0.51155	−21.28	2.37	2.13	
SCB-Gn-GAV	7.425	35.958	9.68	1.88	0.11761	0.51161	−20.15	0.63	2.29	
SCB-Ag-ITA2	7.383	35.750	89.415	14.74	0.0996	0.51121	−27.84	−2.47	2.46	4
SPP-Gn-PDS	7.462	35.868	27.8	3.97	0.08644	0.51087	−34.41	−5.66	2.61	4
CA-42	8.028	35.667	14.834	2.980	0.1215	0.511541	−21.4	−1.74	2.5	6

3.3.4. *Banded gneiss of Vertentes Complex (SU-541)*

Twenty six analyses were conducted of 26 zircon crystals from sample SU-541. Five analyses have discordant ages greater than 10% and are not considered in the following discussion. From the twenty one concordant or slightly discordant ages, eighteen are from grains with Th/U ratios greater than 0.1, among which three distinct age groups may be recognized (Fig. 5b). The first group comprises three analyses with $^{207}Pb/^{206}Pb$ ages between 2.16 Ga and 2.23 Ga that cannot be clustered to give a mean age. It is possible that these analyses are from xenocrystic grains, in which case their $^{207}Pb/^{206}Pb$ ages represent minimum estimates of their crystallization ages.

The second age group is formed by a cluster of five analyses (#006-Z04, #035-Z22, #040-Z25, #41-Z26, #042-Z27) that have $^{207}Pb/^{206}Pb$ ages varying from 2.08 to 2.12 Ga and gave a weighted average mean age of 2096 ± 23 Ma. The dated grains are characterized by well-developed concentric oscillatory zoning (Fig. 5b) and, therefore, the age of 2096 Ma is interpreted as the age of crystallization of the protolith.

The third group is formed by ten analyses that align along a discordia line and have an upper intercept age of 2044 ± 27 Ma (Fig. 5b). In spite of the high MSWD (=15), this age is considered representative since the most concordant analyses (five grains) gave a weighted average of 2060 ± 14 Ma, which overlap within error with the discordia age. The age of 2044 Ma could be interpreted either as the minimum crystallization age of the protolith or as resulting from metamorphic disturbance. The latter interpretation is favored in view of: (a) the age of 2048 ± 22 Ma obtained in a grain with low Th/U ratio (0.08; #039-Z24) and, therefore, of presumed metamorphic origin; (b) the grains show faint oscillatory zoning and embayments cutting the concentric zoning (Fig. 5b), suggesting, respectively, homogenization and dissolution during metamorphism.

Analysis 039-Z24 and two grains with low Th/U (#023-Z15 and #029-Z18) define another discordia with an upper intercept of 1986 ± 38 Ma. The significance of this age is uncertain but it may correspond to another metamorphic event (see *Discussion*).

3.3.5. *Felsic gneiss (SU-515)*

Twenty nine analyses were conducted on 29 zircons from sample SU-515. Most analyses are discordant. Six analyses from grains with Th/U ratio >0.18 are less than 5% discordant. One of these (analysis #032-Z23) yielded a $^{207}Pb/^{206}Pb$ age of 2106 ± 66 Ma, and possibly was obtained in a xenocrystic grain present in the zircon population. The other five analyses (#029-Z20, #026-Z17, #005-Z03, #016-Z10, 027-Z18) can be clustered to give a weighted mean $^{207}Pb/^{206}Pb$ age of 1981 ± 23 Ma (Fig. 5c). This age is the preferred estimate for the crystallization of the protolith because the analyzed zircons are euhedral and show well-

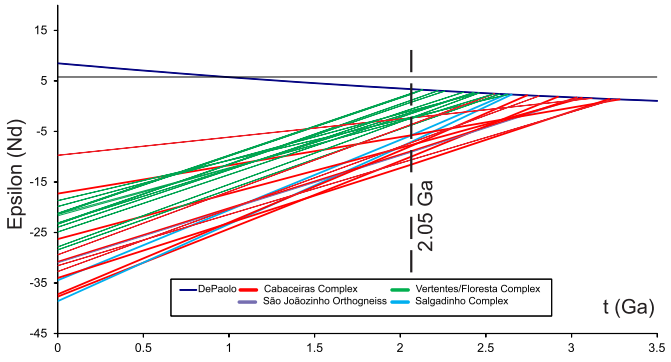

Fig. 6. Nd evolution paths versus age for Paleoproterozoic basement rocks from eastern Borborema.

Table 3
Major and trace element geochemistry of orthogneissic samples from the eastern Central Domain of Borborema Province. *Data from Neves and Alcantara (2010).

Sample	GL-215	GL-18B	GL-024	GL-476	RS-46	RS-396A	RS-408	GL-485	GL-487	RS-424	RS-234	CIV−30B*	SU-497	SU-503	RS-155	RS-215	RS-218	RS-323	RS-165	RS-373	RS-250	CIV-61*
Unity	Cabaceiras											Salgadinho										
Major elements (wt.%)																						
SiO_2	67.45	72.37	70.22	71.35	72.91	71.63	65.67	67.05	70.48	72.82	75.79	71.68	74.63	70.91	68.27	73.14	68.78	70.27	66.11	65.22	47.52	71.09
Al_2O_3	15.3	15.09	15.64	15.37	14.17	15.51	16.24	16.29	12.78	12.17	11.84	14.32	13.02	14.73	16.28	13.81	15	14.12	16.76	15.91	16.96	15.55
Fe_2O_3	2.8	1.14	1.77	1.66	1.67	1.97	3.93	2.69	4.82	4.15	2.68	3.42	1.59	3.94	3.43	2.97	3.8	4.01	4.09	4.94	12.17	0.79
MnO	0.04	0.02	0.02	0.02	0.02	0.02	0.05	0.03	0.06	0.04	0.07	0.09	0.04	0.07	0.06	0.07	0.07	0.08	0.08	0.09	0.16	0.02
MgO	1.67	0.24	0.62	0.36	0.56	0.48	1.61	1.07	0.47	0.67	0.21	0.73	0.35	0.84	0.94	0.86	1.61	1.37	1.25	1.97	5.31	0.27
CaO	2.15	1.2	1.89	1.77	1.42	2.23	3.49	2.16	1.92	1.29	1.02	2.61	1.23	3.08	3.87	2.56	3.44	3.57	4.36	3.96	8.06	1.4
Na_2O	3.85	4.19	4.3	3.76	3.44	4.75	4.5	4.52	2.51	2.28	2.72	4.02	3.22	4.43	4.24	3.68	3.78	3.34	4.35	3.86	2.04	3.99
K_2O	5.55	5.05	4.43	4.88	5.08	2.7	2.9	4.72	5.3	5.41	4.68	2.1	4.82	1.11	1.8	2.29	2.43	2.21	1.81	2.59	4.26	5.31
TiO_2	0.48	0.18	0.32	0.24	0.2	0.23	0.46	0.44	0.64	0.56	0.22	0.27	0.25	0.32	0.32	0.27	0.35	0.33	0.35	0.4	1.13	0.11
P_2O_5	0.27	0.06	0.12	0.05	0.09	0.08	0.16	0.18	0.16	0.11	0.04	0.113	0.06	0.08	0.14	0.08	0.1	0.11	0.14	0.12	0.86	0.049
LOI	0.1	0.3	0.4	0.4	0.1	0.3	0.4	0.5	0.6	0.5	0.4	0.5	0.5	0.3	0.5	0.1	0.4	0.4	0.5	0.7	0.9	0.7
Total	99.47	99.84	99.73	99.85	99.85	99.89	99.71	99.67	99.73	99.81	99.67	99.85	99.7	99.81	99.81	99.82	99.76	99.82	99.79	99.76	99.37	99.26
Trace elements (ppm)																						
Ni	26.4	1.3	5.9	2				12	4.4		0.9	<20	<20	4.9	2	1.3	14.8	1.9	6.7	5.8	19.1	<20
Co					3.3	2.6	7.9			5.6	1.1	70.9	33.1	31.3	4.5	4.3	9.2	7.5	7.4	10.5	28.3	51.9
Sc	7.6	1.5	4.1	2.7	3	2	7	6.7	6.1	8	4	7	3	11	5	7	8	11	8	11	25	2
V	35	<8	18	18				28	24		<8	21	9	25	18	34	53	70	40	74	217	<8
Cu	20.8	1.7	7	4.3	12.9	8.9	5.7	10.8	3.3	3.8	11.9	4.9	1	3.8	2.8	3.9	2.6	4.6	12.1	5.2	107	27.6
Pb	18.4	7.5	3.9	6.2	2.3	2.1	4.8	5.2	3.6	4	6.1	0.7	6.5	0.6	3.1	1.6	2.9	1.4	1.6	2.4	6	28.7
Zn	44	37	35	35	29	41	78	52	60	41	40	51	23	34	51	43	51	38	65	57	116	13
Mo	0.7	<0.1	<0.1	<0.1	2.6	<0.1	0.2	<0.1	0.5	3.3	0.2	0.5	0.4	0.8	0.1	3.8	0.1	2.9	0.8	2.3	0.7	0.1
Rb	193	148.3	115.4	123.8	101.9	106.4	76.2	182.8	91.9	220.9	78.1	57.1	124	25.8	72.2	60.5	73.5	71	47.7	76.4	156.4	92
Ba	2504	804	1133	654	588	460	952	1384	1454	769	1731	903	1969	733	602	924	947	900	643	879	2689	4820
Sr	1422.3	282.3	548.3	280.2	200.6	290.2	529	656.6	144.9	72.3	127.8	284.4	241.1	450.8	686.8	256	417.1	274.4	580.2	320.5	400.3	1578
Ga	20.6	24.9	20.5	23.2	13.8	20.6	20.8	24.4	19.4	17.5	13.8	15.1	13.1	16.9	18.3	12.9	17.1	13.5	18.2	17.4	24.5	21.5
Ta	1.1	0.3	0.2	0.2	0.1	0.4	0.3	0.4	0.5	1.3	1.3	0.4	0.8	0.2	0.2	0.4	0.6	0.4	0.2	0.6	1.2	0.2
Nb	13.4	3.7	6.4	3.7	3.2	4.9	6.6	8.1	14.7	27.1	14.7	4.1	9.7	3.7	10.4	7.7	9.1	7.8	4.5	11.6	17	6.3
Hf	7.7	4.5	6.3	4.7	4.1	3.4	4.1	7	14.6	15.6	11.1	3	5.3	4.7	4.1	3.6	4.7	3.3	2.3	4.7	3.6	4.8
Zr	262.7	148.8	236.9	147.6	124.5	132.7	158.7	274.6	585.4	574.5	375.2	95.6	171.7	167.1	147.1	127.4	157.3	109.1	89.2	174.2	135.1	115.8
Y	11	2.7	3	3.2	8.9	3.3	4.9	5.6	32.6	72.7	92.6	13.7	17.4	12.4	6.3	14.9	14.4	15	11.3	22	37.9	4.6
Th	28.3	20.1	17.9	19.5	13.5	8	1.3	21.9	5.1	43.3	12.1	2.9	12	3.5	11.2	7.4	9	6.2	3.5	7.5	11.6	14.8
U	5.5	4.1	1	0.8	0.4	1.6	0.6	1.7	0.8	3	3.7	0.3	2.5	0.4	0.7	0.8	2.1	1	0.7	1.2	3.8	2.1
La	84.7	42.2	44	44.3	41	22.8	26.9	59.4	56.4	98.6	67.3	25.4	42.5	25	45.4	30.1	25.1	23.6	20.4	34.1	81.9	24.5
Ce	158.2	64.5	74.9	75.9	76.6	39	47	103.1	105.7	197.4	146.6	30.5	84.3	53.8	81.3	60.1	46.1	45.7	39.9	64.3	167.8	45
Pr	17.32	7.08	7.33	7.66	8.71	4.23	5.28	10.43	12.27	22.15	18.1	4.66	7.95	6.32	8.87	6.39	5.48	4.88	4.82	7.39	20.89	5.01
Nd	57.6	23.4	24	24.8	29.7	13.1	17.7	35.2	49.6	79	67.7	16	26.5	26.2	28.9	21.5	18.7	16.9	17.9	25.3	81.7	17.9
Sm	8.13	3.19	3.18	3.25	4.81	2.21	2.87	4.36	8.55	14.56	13.55	2.73	4.27	4.55	3.65	3.58	3.63	2.64	2.99	4.59	14.17	3.03
Eu	1.77	0.64	0.91	0.79	0.78	0.59	0.83	1.16	2.66	1.77	1.67	0.74	0.98	1.1	1.22	0.71	0.79	0.65	0.87	1.01	3.01	0.91
Gd	4.37	1.81	1.66	1.94	3.4	1.26	1.86	2.8	7.85	13.13	12.65	2.32	3.34	3.5	2.16	2.72	2.86	2.14	2.26	4	10.3	1.98
Tb	0.53	0.19	0.17	0.21	0.43	0.16	0.26	0.31	1.22	2.25	2.37	0.38	0.52	0.51	0.28	0.46	0.47	0.37	0.35	0.64	1.45	0.25
Dy	2.28	0.59	0.73	0.79	1.91	0.7	1.02	1.38	6.76	13.08	14.07	2.06	2.97	2.61	1.2	2.33	2.34	2.09	1.88	3.64	7.19	1.04
Ho	0.36	0.09	0.1	0.1	0.34	0.11	0.19	0.19	1.34	2.6	3.29	0.39	0.6	0.45	0.22	0.51	0.51	0.46	0.38	0.81	1.25	0.15
Er	0.8	0.16	0.26	0.23	0.77	0.26	0.49	0.51	3.84	7.4	10.23	1.09	1.87	1.04	0.54	1.53	1.53	1.45	1.08	2.35	3.44	0.32
Tm	0.14	0.03	0.03	0.03	0.13	0.04	0.07	0.07	0.56	1.12	1.67	0.17	0.29	0.14	0.08	0.24	0.22	0.24	0.18	0.35	0.51	0.03
Yb	0.84	0.17	0.17	0.2	0.65	0.26	0.48	0.39	3.26	6.62	11.61	1.11	2.08	0.88	0.53	1.62	1.5	1.72	1.02	2.56	3.24	0.29
Lu	0.11	0.02	0.03	0.03	0.1	0.04	0.07	0.06	0.46	0.84	1.73	0.17	0.31	0.13	0.09	0.24	0.23	0.28	0.16	0.38	0.48	0.04
∑REE	337.15	144.07	157.47	160.23	169.33	84.76	105.02	219.36	260.47	460.52	372.54	87.72	178.48	126.23	174.44	132.03	109.46	103.12	94.19	151.42	397.33	100.45

Sample	GL-093A	GL-108	GL-152	GL-339	GL-446	GL-447	GL-479	GL-480	GL-481	GL-093A	GL-108	GL-152
Unity	*São Joaozinho*											
Major elements (wt.%)												
SiO_2	65.53	72.47	68.87	62.07	57.03	63.2	69.21	68.51	66.76	61.68895	61.32074	60.95252
Al_2O_3	16.07	13.52	13.32	17.72	20.65	17.07	14.62	15	14.19	15.5921	15.57502	15.55795
Fe_2O_3	5.13	3.87	5.3	5.37	5.11	5.86	4.24	4.29	6.01	5.701429	5.755857	5.810286

MnO	0.08	0.05	0.08	0.08	0.07	0.09	0.06	0.06	0.09	0.108381	0.111345	0.11431			
MgO	0.3	0.48	0.72	0.2	0.7	0.25	0.37	0.4	0.21	1.901905	2.021476	2.141048			
CaO	2.85	2.03	2.63	3.19	6.53	3.2	2.57	2.2	3.78	3.698667	3.749167	3.799667			
Na_2O	4.4	3.74	3.29	5.11	6.03	4.4	3.71	3.7	3.25	3.406095	3.339024	3.271952			
K_2O	4.41	3.13	3.82	4.8	2.7	4.83	3.98	4.73	4.66	5.195524	5.297631	5.399738			
TiO_2	0.35	0.37	0.6	0.46	0.5	0.39	0.36	0.41	0.44	0.707619	0.730405	0.75319			
P_2O_5	0.09	0.11	0.22	0.14	0.2	0.11	0.12	0.14	<0.01	0.148214	0.149762	0.15131			
LOI	0.3	0	0.8	0.2	0	0	0.4	0	0.1	0.98	1.0425	1.105			
Total	99.5	99.76	99.65	99.33	99.51	99.4	99.65	99.44	99.49	99.82	99.76	99.81			
Trace elements (ppm)															
Ni	2.4	1.8	3.1	0.8	2.1	1.3	1.3	2.1	1.5	<20	15.3	5.7			
Co	2.9	4.3	6.3	2.6	5.6	2.7	4	4.1	2.9	49.6	12.6	30.8			
Sc	9	7	10	12	8	11	8	6	10	12	13	15			
V	<8	19	23	<8	35	23	13	16	33	<8	55	82			
Cu	7	4.8	6.5	1.6	2.6	1.6	5.4	3.7	2.5	55.2	25.7	1.1			
Pb	4.7	1.4	5.7	1.9	3.3	5.4	5.5	6.6	2.1	2.8	5.1	0.9			
Zn	86	66	91	57	14	102	77	92	81	35	60	71			
Mo	0.6	0.6	1	0.4	0.2	<0.1	0.9	0.5	0.6	2.7	1.2	0.5			
Rb	77.2	75.9	98.2	61.2	40.3	68.4	72.9	68	71.6	22.4	69.5	39			
Ba	3042	1339	1275	3731	1517	3202	1890	2727	2900	542	1045	582			
Sr	303.5	170.5	203.6	392.9	991.3	351.3	251.5	268	386	386.8	471.3	388.4			
Ga	25.6	19.7	20.4	26.3	26.3	21.8	25.4	26.5	28.6	17.7	20	16.9			
Ta	0.5	0.5	1.3	0.4	1.5	0.8	0.6	0.6	0.5	0.2	0.2	0.4			
Nb	14.3	9.8	19	10.7	33.7	18.4	12.8	20	15.3	5.3	7.1	6.1			
Hf	13	9.4	11.3	19.1	14.1	15	10.4	14.5	19.4	5.5	5.1	3.7			
Zr	528.3	319.4	426.9	791.6	534.5	655.3	399.2	556.4	806.2	222.5	207	110.4			
Y	38.8	42.2	70.1	37.9	49.4	46.9	52.9	67.1	37.4	11.6	15.8	14.7			
Th	8.4	4.2	12.5	6.1	19.3	10.3	7.6	9.2	9.2	3.5	4.1	5.2			
U	1.6	1.1	2.5	2.2	4	1.7	2.4	1.5	1.6	0.9	0.4	0.6			
La	94.1	39.4	68.1	84.9	131.4	112.3	69.4	111.8	132.1	15.5	47.4	16.1			
Ce	188.4	82.3	142.4	158.9	251.7	223	140.3	221.5	256.8	35.5	88.5	34.1			
Pr	22.12	10.47	17.3	17.93	27.2	25.97	16.35	25.84	27.83	4.1	9.56	3.93			
Nd	84.4	39.8	69.4	63.5	88.7	94.8	63.4	101.9	95.1	16.3	35.7	16.1			
Sm	13.01	8.65	13.4	10.31	13.55	15.61	10.74	16.6	14.11	2.92	5.21	3.19			
Eu	2.89	1.39	1.73	4.56	2.7	3.48	2.05	3.12	3.85	1.13	1.16	0.84			
Gd	9.66	8.17	13.06	8.09	11.34	12.44	10.02	15.11	10.52	2.35	3.55	2.81			
Tb	1.48	1.33	2.17	1.26	1.64	1.69	1.61	2.34	1.46	0.35	0.51	0.46			
Dy	8.06	7.5	12.94	7.18	9.35	8.72	9.59	13.44	7.35	2	2.83	2.47			
Ho	1.47	1.53	2.61	1.38	1.86	1.8	1.97	2.6	1.4	0.46	0.54	0.49			
Er	4.24	4.36	7.53	4.01	5.04	4.71	5.63	7.08	4.27	1.48	1.5	1.5			
Tm	0.63	0.68	1.2	0.64	0.8	0.77	0.83	1.06	0.6	0.24	0.24	0.21			
Yb	4.28	4.62	7.49	4.02	4.81	4.51	5.11	6.21	4.35	1.81	1.6	1.54			
Lu	0.67	0.7	1.08	0.68	0.68	0.68	0.72	0.93	0.72	0.3	0.26	0.23			
∑REE	435.41	210.9	360.41	367.36	550.77	510.48	337.72	529.53	560.46	84.44	198.56	83.97			

Sample	VAN-03*	VAN-29*	VAN-58*	VAN-59*	VAN-52a*	VAN-53*	SU-551	RS-128	RS-190	RS-326	RS-328	RS-426	VAN-43*	VAN-45*	RS-145	SU-515
Unity	Vertentes															
Major elements (wt.%)																
SiO_2	66.42	58.44	64.15	66.04	57.7	63.12	57.19	58.16	53.87	58.55	61.32	63.86	69.78	69.95	70.3	73.72
Al_2O_3	15.48	16.49	14.65	15.61	15.03	16.51	20.19	17.02	18.19	16.5	16.82	16.69	14.85	15.47	15.01	13.45
Fe_2O_3	5.67	7.99	5.14	3.3	6.71	5	4.85	7.07	8.81	6.68	5.43	5.04	2.29	1.79	2.69	1.67
MnO	0.1	0.1	0.11	0.07	0.13	0.1	0.07	0.11	0.13	0.1	0.1	0.09	0.07	0.05	0.05	0.06
MgO	1.78	3.12	1.21	0.63	1.96	1.85	1.57	2.95	3.42	4.12	1.71	1.7	0.96	0.48	0.53	0.33
CaO	2.54	4.23	2.66	1.96	4.6	4.45	5.55	5.89	6.25	5.83	3.68	3.86	1.36	1.44	2.43	1.76
Na_2O	3.45	2.97	3.74	4.39	2.74	4.22	4.32	4.04	4.4	3.31	4.76	3.88	4.45	4.74	3.75	3.49
K_2O	3.03	3.74	5.78	5.79	7.69	2.59	3.77	2.26	2.68	3.08	4.03	3.32	5.05	4.67	3.87	4.22
TiO_2	0.55	0.84	0.65	0.41	1.03	0.52	0.65	0.75	0.98	0.58	0.44	0.61	0.2	0.22	0.26	0.19
P_2O_5	0.103	0.471	0.177	0.129	0.347	0.275	0.24	0.32	0.46	0.25	0.23	0.24	0.135	0.094	0.1	0.06

(*continued on next page*)

Table 3 (*continued*)

Sample	VAN-03*	VAN-29*	VAN-58*	VAN-59*	VAN-52a*	VAN-53*	SU-551	RS-128	RS-190	RS-326	RS-328	RS-426	VAN-43*	VAN-45*	RS-145	SU-515
Unity	Vertentes															
LOI	0.7	1.3	0.7	0.6	1.1	1	1.1	1	0.4	0.6	0.7	0.4	0.2	0.4	0.8	0.9
Total	99.84	99.67	98.99	98.94	99.04	99.64	99.51	99.6	99.62	99.61	99.19	99.67	99.36	99.29	99.75	99.85
Trace elements (ppm)																
Ni	45	<20	32	45	<20.	<20		9.4	16.2	26.5	5.9	5.1	28	22	1.6	<20
Co	49.2	61.7	60.2	84.1	81.9	39.5	62.9	17.8	21.9	22.1	11.6	11.1	50.7	96.1	3.8	21.6
Sc	13	15	11	6	15	9	11						6	5		3
V	77	85	38	17	53	33	46	84	98	99	38	45	28	21	11	14
Cu	26.6	32.7	10.9	1.1	31	13.7	10.2	22.3	24.9	5.4	10.3	4.7	2.9	1.5	10.8	2.7
Pb	2.1	6.9	23.8	20.6	24.6	3	6.4	2.5	5.3	5.4	21.4	5.4	26.7	19.9	5.6	8
Zn	83	95	61	27	27	61	62	66	79	42	77	67	33	54	40	40
Mo	1	0.5	0.7	0.4	0.2	0.3	0.9	0.5	0.6	1.5	0.6	0.1	0.3	0.3	3.1	0.9
Rb	145.9	90.1	98.1	85.2	145.4	72.9	89	45	86.8	77.6	70.9	141.6	110.8	72.7	93.4	112.2
Ba	669	1658	5243	5457	5959	1576	2182	1348	1236	1499	4223	1648	3635	3597	1180	886
Sr	308.1	603.7	2272	2759	970.3	844.8	946.1	906.5	879	666.4	1815.9	750.3	1183	1591	536.1	174.2
Ga	20.8	17.8	18.9	19.1	14.1	19.9	23.3	18.4	22.2	17.2	20.3	20.2	14.2	19.1	17	19
Ta	0.9	1	0.9	0.9	1.2	0.3	0.5	0.3	0.7	0.3	0.5	0.7	<0.1	0.3	0.1	1
Nb	10.7	13.8	14.5	13.5	17.4	5.1	10.9	6.8	12.2	8.4	11.3	13.2	5	7.8	5.1	11.4
Hf	5.5	4.7	7.7	7.7	6.6	3.3	8.1	4	4.9	6	5.7	4.3	3.6	4.8	4	4.5
Zr	177.5	164.6	313.8	293.7	253.5	136.6	316.1	152.8	195	220.9	241.1	154.9	117	139.5	136	149.6
Y	21.2	24.9	29.8	21.2	24.4	10.8	16.8	15.5	23.7	14.3	16.2	11.8	15.8	7.6	7	11
Th	16.4	24.7	8.7	10.4	6.7	5.8	8.8	1.1	5.4	1.6	11.1	2.6	5.9	6.4	7.5	11.8
U	3	2.8	1.2	1	1.7	0.6	1.9	0.3	1.3	0.5	2.7	0.8	1.2	0.9	0.6	1.8
La	44.3	74.7	108.2	93.5	54.2	49	44.5	29.7	45.3	33.2	72.7	49.8	30.7	24.6	30.7	33
Ce	90	155.1	188.4	157.8	119.8	76.8	89.4	60.4	92.5	62.8	136	92.1	53.7	46.8	55.1	62.7
Pr	10.69	16.47	23.51	19.02	16.22	9.02	9.73	7.62	11.56	7.59	15.77	10.17	5.98	5.26	5.85	6.44
Nd	39.3	59.8	81.8	63.5	58.4	29.4	36.6	30	42.1	28	55.7	37.1	18.7	18.6	19.8	20.9
Sm	7.51	9.83	13.52	10.86	9.63	4.49	5.91	5.13	7.97	5.13	8.45	5.23	3.19	3.02	2.57	3.33
Eu	1.11	2.18	3.31	2.72	2.55	1.74	1.97	1.54	1.85	1.44	2.05	1.53	0.96	1.08	0.92	0.63
Gd	6.06	6.58	7.66	5.72	5.72	2.64	4.65	3.91	5.73	3.7	5.26	3.63	2.32	1.78	1.62	2.26
Tb	0.88	0.97	1.22	0.9	0.97	0.41	0.63	0.57	0.86	0.55	0.68	0.46	0.43	0.32	0.22	0.36
Dy	4.2	4.72	5.56	3.88	4.48	1.91	3.21	2.97	4.44	2.74	3.09	2.08	2.28	1.65	1.28	2
Ho	0.72	0.78	1.01	0.68	0.8	0.34	0.6	0.54	0.84	0.51	0.58	0.38	0.4	0.28	0.24	0.37
Er	2.15	2.31	2.37	1.84	2.14	0.95	1.59	1.41	2.21	1.47	1.58	0.95	1.12	0.7	0.65	1.11
Tm	0.36	0.34	0.39	0.24	0.27	0.15	0.24	0.22	0.33	0.21	0.23	0.16	0.16	0.1	0.11	0.17
Yb	2.17	2.19	2.21	1.54	1.79	0.92	1.54	1.33	2.02	1.35	1.54	0.91	0.92	0.55	0.69	1.13
Lu	0.34	0.32	0.36	0.26	0.26	0.14	0.21	0.2	0.3	0.2	0.23	0.14	0.14	0.08	0.12	0.18
∑REE	209.79	336.29	439.52	362.46	277.23	177.91	200.78	145.54	218.01	148.89	303.86	204.64	121	104.82	119.87	134.58

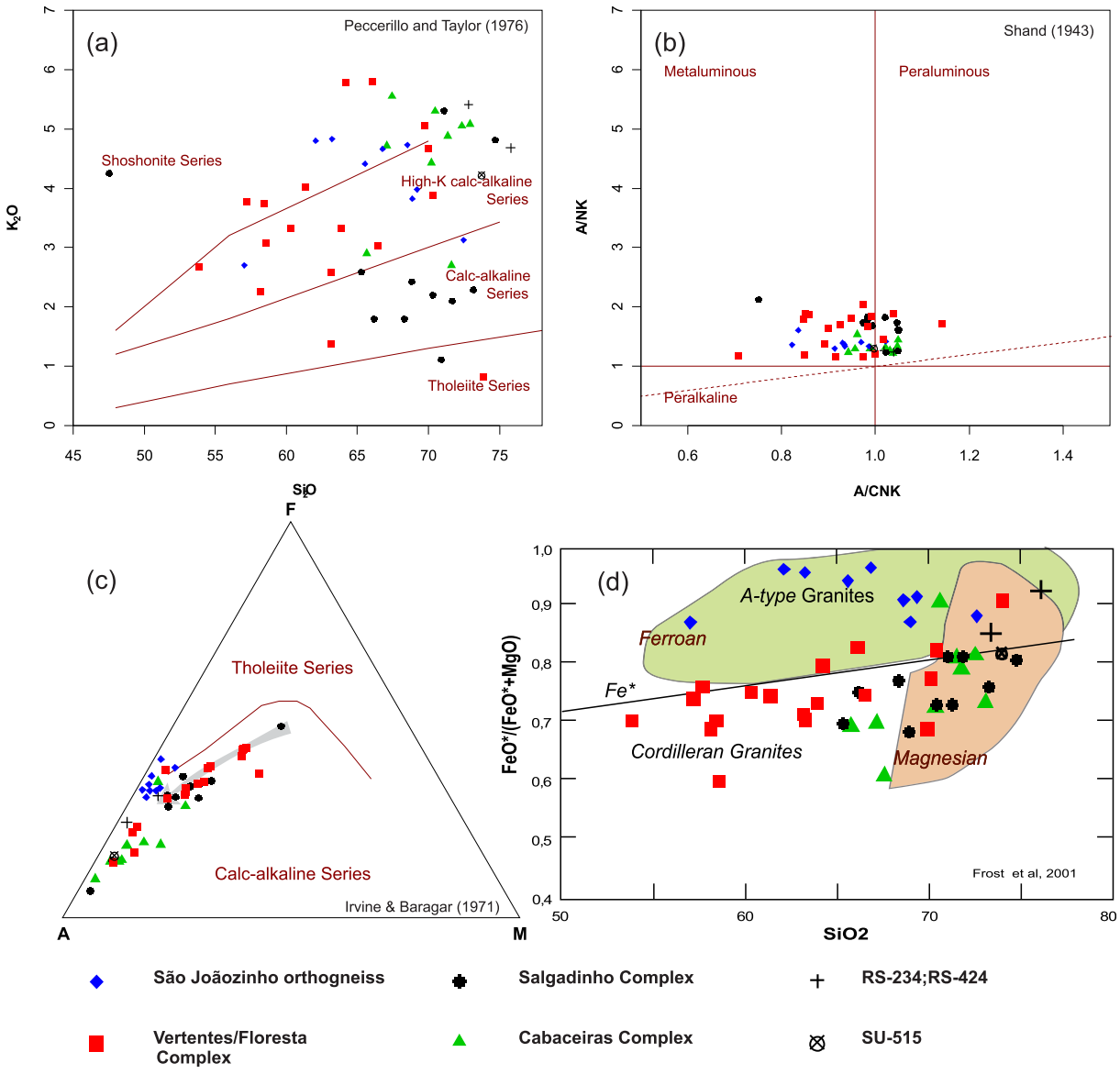

Fig. 7. Major element characteristics of orthogneisses. (a) K_2O vs. silica diagram. Fields of magmatic series from Peccerillo and Taylor (1976). (b) Alumina saturation. (c) AFM diagram. Fields of magmatic series from Irvine and Baragar (1971). (d) FeOt/(FeOt + MgO) against SiO_2 diagram showing the fields for magnesian and ferroan rocks and the range of compositions of Cordilleran and A-type granites (Frost et al., 2001).

developed oscillatory zoning (Fig. 5c). The upper intercept of the discordia (1930 ± 49 Ma) obtained by regression of all data show large MSWD (11.8) but can be considered with caution to result from lead loss during a metamorphic and/or magmatic event around 1.93 Ga. This interpretation is supported by two analyses ((#031-Z18 and #031-Z22) with low discordance that gave ages of 1929 ± 25 Ma and 1925 ± 22 Ma. In the first, the laser beam shot the core of a partially resorbed grain and, in the latter, a large overgrowth rim (Fig. 5c).

3.4. Sm–Nd isotopic data

Sm–Nd data are presented in Table 2, including those obtained in the present study and results from the literature, and a ε_{Nd} versus age diagram is shown on Fig. 6. An age of 2050 Ma was used for the calculation of $\varepsilon_{Nd}(t)$ values. In the Cabaceiras Complex, the dated sample GL-476 yielded ε_{Nd} value of −7.92 and Nd T_{DM} model age of 2.74 Ga. Three other samples and previous results also yield negative ε_{Nd} values, with Archean model ages ranging from 2.5 to 3.3 Ga. These results suggest participation of a Meso- to Neoarchean component in the genesis of this complex. Two analyses of the Salgadinho Complex gave similar Nd model ages of c. 2.6 Ga. Sample GL-479 from the São Joãozinho augen gneiss has Nd T_{DM} model age of 3.03 Ga and ε_{Nd} value of −8.43, which suggest derivation from reworked Mesoarchean crust. Banded gneisses of the Vertentes Complex have in general younger model ages than the granitic gneisses, mostly ranging from 2.2 to 2.5 Ga and slightly negative to positive ε_{Nd} values, indicating derivation from more juvenile sources.

4. Geochemistry

Chemical analyses were performed at Acme Analytical Laboratories Ltd. in Canada. Major elements were determined using inductively coupled plasma-emission spectrometry with a detection limit of 0.01% and precision of ±0.1%. Trace and rare earth elements were analyzed using inductively coupled plasma-mass

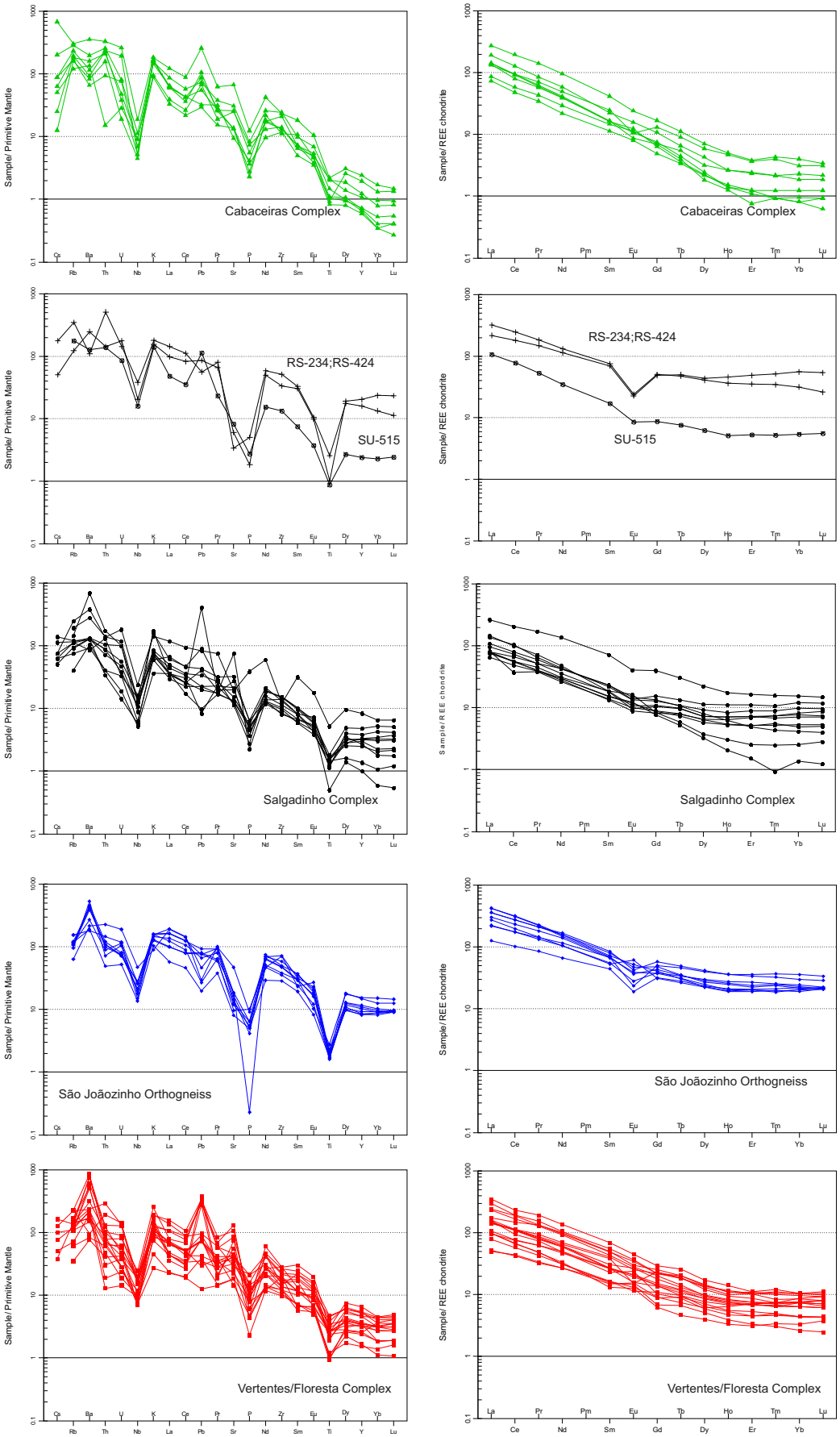

Fig. 8. (left) Spider diagrams of trace elements abundances normalized to primitive mantle (McDonough and Sun, 1995). (right) Rare earth elements abundances normalized to chondrite (Boynton, 1984).

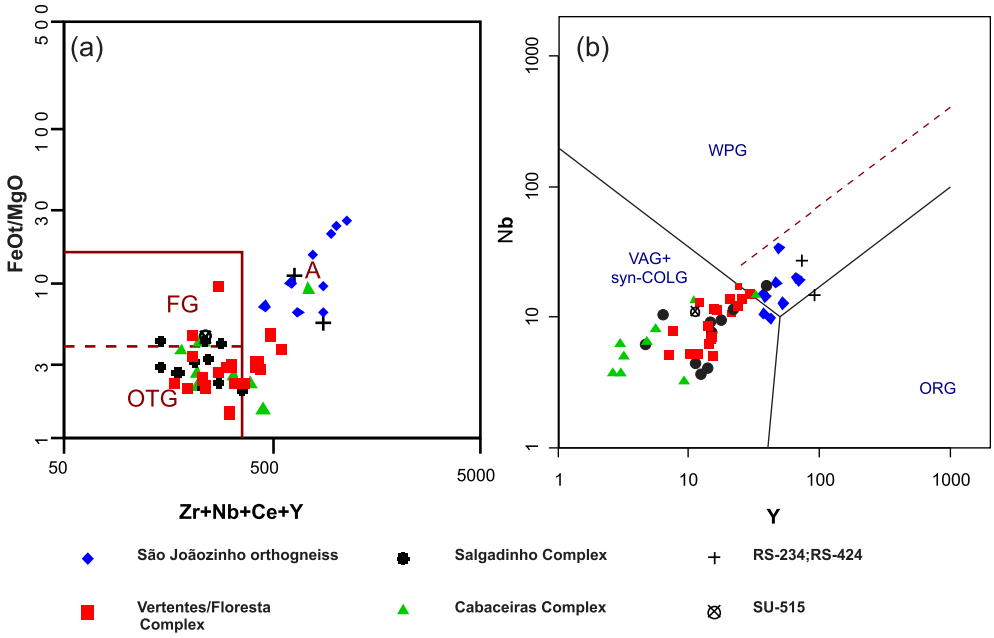

Fig. 9. (a) FeOt/MgO versus Zr + Nb + Ce + Y discrimination diagram of Whalen et al. (1987). A: A-type granites; FG: fractionated felsic granites; OFG: unfractionated I, M and S granites. (b) Nb versus Y discrimination diagram of Pearce et al. (1982). WPG: within-plate granite; ORG: ocean ridge granite; VAG + Syn-COLG: volcanic arc- and collision-related granites.

spectrometry (ICP-MS) with detection limits between 0.01 and 0.5 ppm and precision of ±5%. Diagrams displaying the geochemical variability of the studied rocks were constructed using PetroGraph (Petrelli et al., 2005) and the latest version of open source software GCDkit 3.0 (Janoušek et al., 2006).

4.1. Migmatitic orthogneisses

The SiO_2 contents of samples from the Cabaceiras and Salgadinho units range from 65 to 74 wt.% (Table 3; Fig. 7a). Harker diagrams (not shown) exhibit low dispersion for most elements, indicating that, in spite of migmatization, significant mobility did not occur. The samples are metaluminous to slightly peraluminous (Fig. 7b) and plot in the field of magnesian granites (Fig. 7d). They follow the calc-alkaline trend in the AFM diagram (Fig. 7c), with samples of Cabaceiras unit extending closer to the A apex. This feature reflects the higher K_2O content of the Cabaceiras samples as compared with samples from the Salgadinho Complex, as shown in the K_2O versus SiO_2 diagram (Fig. 7a): the first fall in the high-K calc-alkaline field and above this field whereas the latter belong to the medium-K calc-alkaline series.

As far as trace elements are concerned, the Cabaceiras and Salgadinho samples have typical features of calc-alkaline rocks, including high ratios of large ion lithophile elements (LILE) to high field strength elements (HFSE) and negative Nb, P and Ti anomalies (Fig. 8). The main distinction between the two units is the higher contents of heavy rare earth elements (heavy REEs) and Y in the Salgadinho Complex (Fig. 8). The Salgadinho samples show moderate fractionation of the REEs, with a rapid decrease from La to Sm and a flattened pattern in the region of the heavy REE. In the Cabaceiras samples the REE patterns exhibit strong fractionation, with $(La/Yb)_N$ up to 200. In both cases, Eu negative anomalies are small or negligible. In tectonic discrimination diagrams, the samples plot in the field for volcanic arc granites (Fig. 9), according with the generally accepted setting for generation of calc-alkaline magmas (e.g., Brown, 1977; Barbarin, 1999; Frost et al., 2001).

In sparkling contrast with the Salgadinho and Cabaceiras complexes, the 2.18 Ga-old sample RS-234 and another sample of the same unit have high contents of heavy REEs, Y and Nb and low values of Sr and Eu (Table 3). These features make that the samples plot on the within-plate field in tectonic discrimination diagrams (Fig. 9). The samples exhibit chondrite normalized REE patterns characterized by well-marked negative Eu anomalies and a flat pattern from Gd to Lu (Fig. 8). These characteristics are typical of A-type granites (e.g., Whalen et al., 1987; Eby, 1992; Frost et al., 2001).

4.2. São Joaozinho augen gneiss

Samples of the São Joaozinho orthogneiss are metaluminous and ferroan (Fig. 7), and plot in the within plate field in tectonic discrimination diagrams (Fig. 9). The chondrite normalized REE patterns show La_N/Yb_N ratio <20, with fractionated LREE and flat HREE patterns, and $(Eu/Eu^*)_N$ between 0.40 and 0.97 (Fig. 8). The primitive mantle normalized multielemental diagrams show smaller LILE/HFSE fractionation than the Salgadinho and Cabaceiras units, with smaller negative anomaly of Nb, and stronger depletion in P and Ti and positive peaks in La and Zr. These features are similar to those of A-type granites.

4.3. Banded gneisses (Vertentes Complex)

Samples of the Vertentes Complex mainly show silica contents varying from 54 to 66 wt.%. Four samples with $SiO_2 \geq 70$ wt.% probably incorporated a large proportion of the felsic bands, which is difficult to avoid given the generally fine banding. The samples are metaluminous to slightly peraluminous, plot in the high-K calc-alkaline field in the K_2O versus SiO_2 diagram, and follow the calc-alkaline trend in the AFM diagram (Fig. 7). Chondrite normalized REE patterns are moderately to strongly fractionated $(La/Yb)_N = 12–48$), showing a rapid decrease from La to Sm and a flat profile in the region of the heavy REEs (Fig. 8). Eu anomalies are generally small, with some samples showing negative anomalies and others positive anomalies. In primitive mantle normalized multielemental diagram (Fig. 8), the samples are characterized by negative anomalies of Nb, P and Ti.

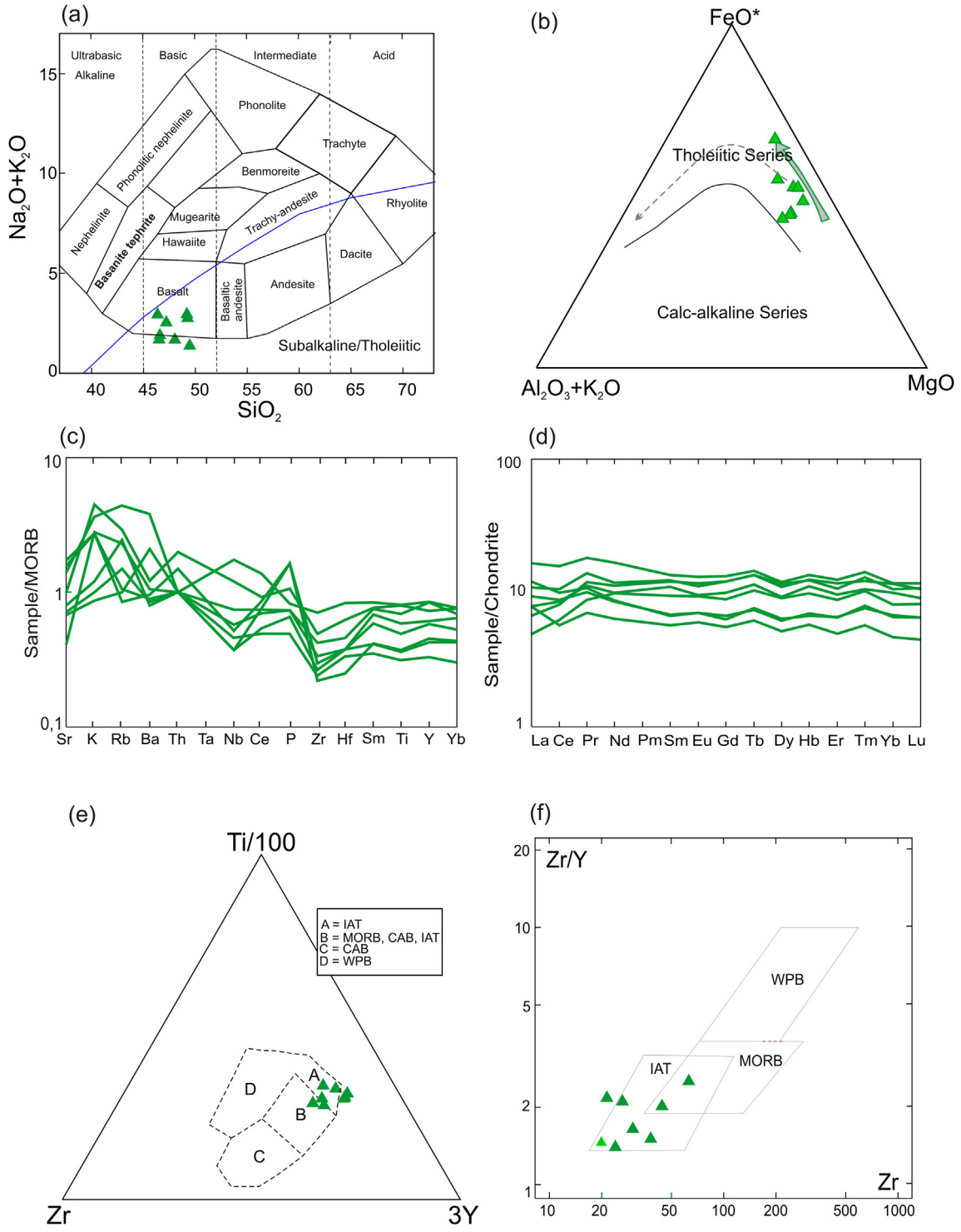

Fig. 10. (a, b) Major elements geochemical characteristics of orthoamphibolites. (a) Total alkalis versus silica (TAS) diagram. Fields from Cox et al. (1979). (b) AFM diagram. Fields of magmatic series from Irvine and Baragar (1971). (c, d) Trace elements geochemical characteristics of orthoamphibolites. (c) MORB-normalized multi-elemental diagram. Normalization values from Pearce (1982). (d) Chondrite-normalized rare earth elements diagram. Normalization values from Boynton (1984). (e, f) Tectonic discrimination diagrams from (e) Pearce and Cann (1973) and (f) Pearce and Norry (1979). CAB: calc-alkalic basalt; IAT: island arc tholeiite; MORB: mid-ocean ridge basalt; WPB: within-plate basalt.

4.4. Orthoamphibolites

The metamafic rocks associated with the Cabaceiras unit display a narrow range of SiO_2 (46–50 wt.%) and $Na_2O + K_2O$ (1.5–3.5 wt.%) contents (Fig. 10). They follow the trend of the tholeiitic series in the AFM diagram; show flat REE patterns, with REE contents about ten times chondrite values; and have high LILE and low HFSE as compared with MORB. In tectonic discrimination diagrams, they plot in the island arc field.

4.5. Felsic gneiss

A single sample of the felsic gneisss unit was analyzed (Table 3). It has high silica and total alkalis contents (73.7 and 7.7 wt.%,

respectively); exhibits a subtle negative Eu anomaly in the chondrite normalized REE diagram (Fig. 8 – sample SU-515), and projects in the field for fractionated granites in the FeO_t/MgO versus Zr + Nb + Ce + Y diagram (Fig. 9a) and in the field of volcanic arc and syncollisional granites in the Nb versus Yb tectonic discrimination diagram (Fig. 9b).

5. Discussion

5.1. Paleoproterozoic magmatic and metamorphic events

Zircons from the dated samples record c. 200 million years of geological history, during which several magmatic and metamorphic events are recognized. The age of 2.18 Ga of sample RS-234 is amongst the oldest found in the Central Domain, where ages

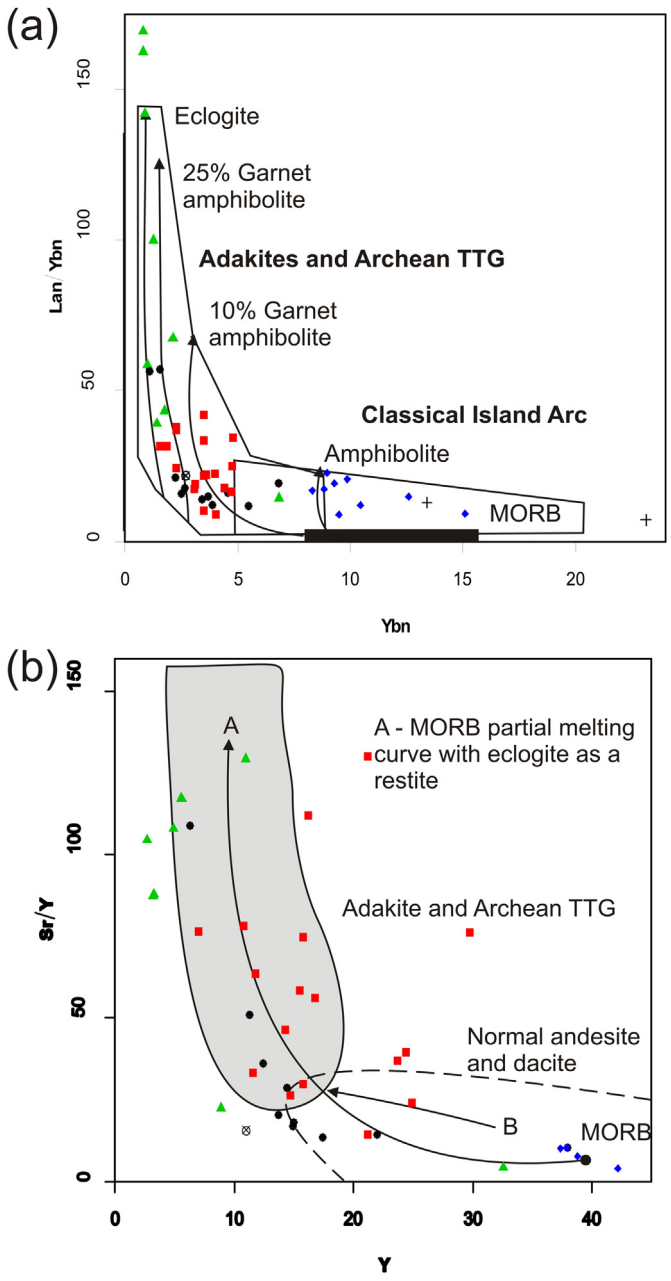

Fig. 11. (a) Sr/Y versus Y (Defant et al., 1991) and (b) $(La/Yb)_N$ versus Yb (Martin, 1986) diagrams showing the fields for adakites and TTGs and for calc-alkaline rocks, and the curves for partial melting of mafic sources leaving garnet at the residue.

younger than 2.15 Ga are more common (Van Schmus et al., 1995, 2011; Neves, 2015, and references cited in these works). This sample and nearby rocks are indistinguishable on field and petrographic basis from the much younger (c. 2.06 Ga) migmatitic orthogneisses of the Salgadinho and Cabaceiras complexes, which demonstrates the need for systematic geochronological and geochemical work in old gneissic terrains.

By large, the most voluminous magmatism in the study area is represented by the emplacement of the protoliths of the Vertentes, Salgadinho and Cabaceiras complexes. The age of the Vertentes complex obtained in this study (2096 ± 23 Ma) falls within the age range (2162-2093 Ma) reported in previous ones (Neves et al., 2006; Brito Neves et al., 2013). These data point out to an important magmatic event with duration of c. 70 Ma. Unexpectedly, the São Joaozinho orthogneiss has an age (2109 ± 15 Ma) that also falls within the range of ages available for the Vertentes Complex, despite their field, petrographic and geochemical dissimilarities. This finding implies that rocks with different geochemical characteristics are not necessarily emplaced in different times during the geological evolution of a given region.

The >40 Ma age difference between the Vertentes Complex and the Salgadinho/Cabaceiras complexes could suggest that magmatism was episodic rather than continuous. However, recent studies suggest that zircons formed in intraoceanic magmatic arcs are less prone to preservation than those generated during continental collisions (Hawkesworth et al., 2010; Dhuime et al., 2012; Cawood et al., 2013), such that this apparent absence of magmatism may be an artefact of the geological record. Another apparent magmatic lull is observed between 2042 ± 11 Ma and 1981 ± 23 Ma, the ages of intrusion of the protoliths, respectively, of the orthoamphibolite and of the felsic gneiss. The latter age is similar within errors to that found (1991 ± 5 Ma) in one sample dated by Neves et al. (2006), attesting intrusion of magmas with clear crustal affinity c. 1.99–1.98 Ga ago.

A metamorphic event at c. 2.06–2.04 Ga is indicated by the 2060 ± 14 Ma weighted average of five concordant ages and the 2044 ± 27 Ma upper intercept age of sample SU-541. A concordant analysis with an age of 2048 ± 22 Ma in a grain with low Th/U and the presence of faint oscillatory zoning and embayments cutting the concentric zoning in other grains (Fig. 5b) also support post-crystallization origin. The age of 2044 Ma of the upper intercept is identical to the one obtained by Neves et al. (2006) in a batch of analyses from another sample of the Vertentes complex whose zircon grains have similar characteristics, thus reinforcing the existence of this metamorphic event.

Sample SU-541 has three grains (two of which with low Th/U ratio) whose analyses have an upper intercept age of 1986 ± 38 Ma. Similar result (1983 ± 20 Ma) was found by Brito Neves et al. (2013) on zircon overgrowths in one of the samples of the Vertentes Complex studied by them. Analyses of four grains with low Th/U ratio from sample RS-423 yielded an upper intercept age of 1996 ± 13 Ma. These data indicate other metamorphic episode around 2.0–1.98 Ga. This time span coincides with the crystallization ages of felsic gneisses in the study area, showing that magmatism and metamorphism were broadly coeval. The geochemical characteristics of sample SU-515 suggest that these events are probably associated with collision. The occurrence or not of yet another metamorphic event around c. 1.93 Ga, as suggested by some analyses of sample SU-515, requires further investigation. Finally, imprints of Brasilano-age metamorphism is evidenced by the low intercept age of 604 ± 20 Ma from sample RS-234.

5.2. Petrogenesis

The dominantly intermediate composition, the metaluminous character, and the relatively high contents of compatible elements

of the Vertentes Complex require that mafic or ultramafic sources are involved on its genesis. Partial melting of mafic protoliths appears unlikely because most dehydration-melting experiments of metabasalts have produced tonalitic to granitic melts rather than dioritic ones (e.g. Rushmer, 1991; Patiño-Douce e Beard, 1995). The high contents of LILE also exclude the depleted mantle as a possible source. Partial melting of an enriched mantle seems to be the better option, with the parental magmas evolving through fractional crystallization. The relatively juvenile Nd model ages suggests little or no interaction with preexisting continental crust.

Similarly to the Vertentes Complex, the Salgadinho and Cabaceiras units have relatively high contents of MgO, CaO and FeO, which exclude sedimentary or felsic igneous rocks as possible sources. On the other hand, ultramafic sources are implausible due to the essentially granitic composition. Derivation from mafic/intermediate sources by either partial melting or fractional crystallization is therefore the most likely hypothesis. In the Salgadinho Complex, the absence of both Eu anomalies and concave-up patterns in the region of the heavy REEs indicate limited participation of plagioclase and amphibole on its genesis. The REE patterns are similar to the samples of the Vertentes Complex, being richer in the heavy REE. This resemblance suggests partial melting of, or differentiation from, sources similar in compositions to the Vertentes Complex through retention/fractionation of mineral phases with low bulk distribution coefficients, such as olivine or pyroxene. In contrast, depletion of heavy REEs in the Cabaceiras unit strongly favors garnet and/or amphibole involvement (Fig. 11), suggesting genesis of the magmas at higher pressures than in the case of the Salgadinho Complex. As a consequence, despite the much higher K_2O content of the Cabaceiras complex as compared with modern adakites and Archean tonalite-trondhjemite-granodiorite (TTG) suites, the high Sr/Y and $(La/Yb)_N$ make the samples to plot in the field for these rocks in the Sr/Y versus Y (Defant et al., 1991) and $(La/Yb)_N$ versus Yb (Martin, 1986) diagrams (Fig.11).

The São Joaozinho orthogneiss has several geochemical affinities with A-type granites, particularly with the metaluminous A-type granites found in the Amazonian Craton (Dall'Agnoll and Oliveira, 2007). Petrogenetic modelling by Dall"Agnoll et al. (1999) suggested that magmas with these characteristics could have been produced by partial melting of clinopyroxene-bearing quartz diorites.

5.3. Tectonic setting, crustal growth and reworking

The geochemistry of the Vertentes, Salgadinho and Cabaceiras complexes is so similar to modern calc-alkaline magmas that generation of the parental magmas in a convergent setting seems to be an inescapable conclusion. The relatively young Nd model age of the Vertentes Complex favors intrusion in an intraoceanic arc rather than in an active continental margin. The presence of older inherited zircons (2.23–2.16 Ga-old) in sample SU-541 could mark the beginning of arc development. In contrast, the Salgadinho and Cabaceiras units, although also displaying subduction-related signature, have essentially granitic composition and slightly peraluminous character, which suggests emplacement in a more evolved setting, probably an active continental margin. The Archean Nd model ages of the Cabaceiras Complex suggest mixing between a juvenile component and an older, crustal, component. Existence of an ancient crustal component is also attested by the Nd model ages of the São Joaozinho orthogneiss and sample RS-234. The island-arc affinity of the orthoamphibolite indicates persistence of a convergent environment until at least 2042 Ma.

If the above inferences are correct, one important point to consider is why rocks with A-type geochemistry are present in a convergent setting. The recent discovery of rifted continental fragments in the Indian Ocean (Torsvik et al., 2013) and the presence of old zircons in juvenile intraoceanic arc terranes (Hargrove et al., 2006) suggest that occurrence of crustal material in oceanic realms may be more common than usually realized. Due to the older age of sample RS-234 (2.18 Ga), it is possible that it belonged to such a fragment that was engulfed by a growing volcanic arc. The age of the São Joaozinho orthogneiss is similar to the age of the Vertentes Complex (c. 2.1 Ga) obtained in this study and poses a different problem. The apparent conundrum of occurrence in the same area of rocks of similar age and different chemical signatures may have several explanations. A-type granites are usually ascribed to intraplate ("anorogenic") settings, but occur in a variety of other settings, the post-collisional one being particularly common (e.g., Jung et al., 1998; Almeida et al., 2002; Bonin, 2007; Li et al., 2014). A-type granites are also described from convergent settings, such as the Lachlan Fold Belt of Australia (King et al., 1997), where their inferred high temperature of formation can be related to extension associated with slab breakoff during arc–arc collision (Yuan et al., 2010; Li et al., 2014), back-arc extension (King et al., 1997; Lister and Foster, 2009), subduction of ocean ridge segments, or delamination of the lower part of thick volcanic arcs. We therefore ascribe the genesis of the São Joãozinho orthogneiss to local extensional conditions in an otherwise convergent setting.

5.4. Geodynamic hypothesis

Our preferred scenario for the evolution of the study area starts with island arc construction around 2.2 Ga, leading to an expressive volcanic arc edifice by 2.13–2.10 Ga (Fig. 12a–d). Strong negative initial ε_{Nd} and Archean Nd model ages for the São Joãozinho orthogneiss and the Cabaceiras Complex indicate that ancient continental material was involved in their genesis. Accordingly, we propose that a microcontinental fragment was assimilated by the growing magmatic arc (Fig. 12 b–d). Production of the parental magmas of the São Joaozinho orthogneiss and of sample RS-234 is attributed to melting of the old crustal component, possibly during periods of back-arc extension associated with slab retreat (Fig. 12c and f), thus explaining their affinity with A-type granites.

It is generally agreed that continents acquire a bulk andesitic composition by internal differentiation and foundering of mafic/ultramafic cumulates (e.g., Kay and Kay, 1993; Jagoutz and Schmidt, 2013; Jagoutz and Behn, 2013). We propose that the Vertentes Complex resulted from the acting of these processes (Fig. 12d and e) and that, by 2.06 Ga, the crust had evolved enough to become intruded by magmas formed at the mantle wedge of the now largely continental magmatic arc (Fig. 12g). Orthogneisses from the Rio Grande do Norte Domain, which outcrop just to the north of the study area (Fig. 1c), have geochemical characteristics indicating intrusion in a continental arc setting (Souza et al., 2007) and ages older than 2.14 Ga (Hackspacher et al., 1990; Van Schmus et al., 1995; Dantas et la., 2004; Souza et al., 2007; Hollanda et al., 2011). We therefore speculate that accretion of the evolving oceanic arc to the active continental margin of the Rio Grande do Norte Domain led to cessation of subduction-related magmatic activity in this domain sometime between 2.15 and 2.13 Ga (Fig. 12d and e).

Although not a universal rule (Arculus, 1994), some arc magmas show a consistent relationship between alkalinity and depth to the Wadati-Benioff zone (e.g., Sakuyama and Nesbitt, 1986). Therefore, greater K_2O and LILE contents and older Nd model ages in the Cabaceiras Complex as compared with the Salgadinho Complex (Figs. 6–8) are assumed to result from northward (present-day coordinates) subduction. Conterminous with intrusion of the protoliths of these complexes, high-temperature conditions were attained at mid crustal levels, being responsible for the

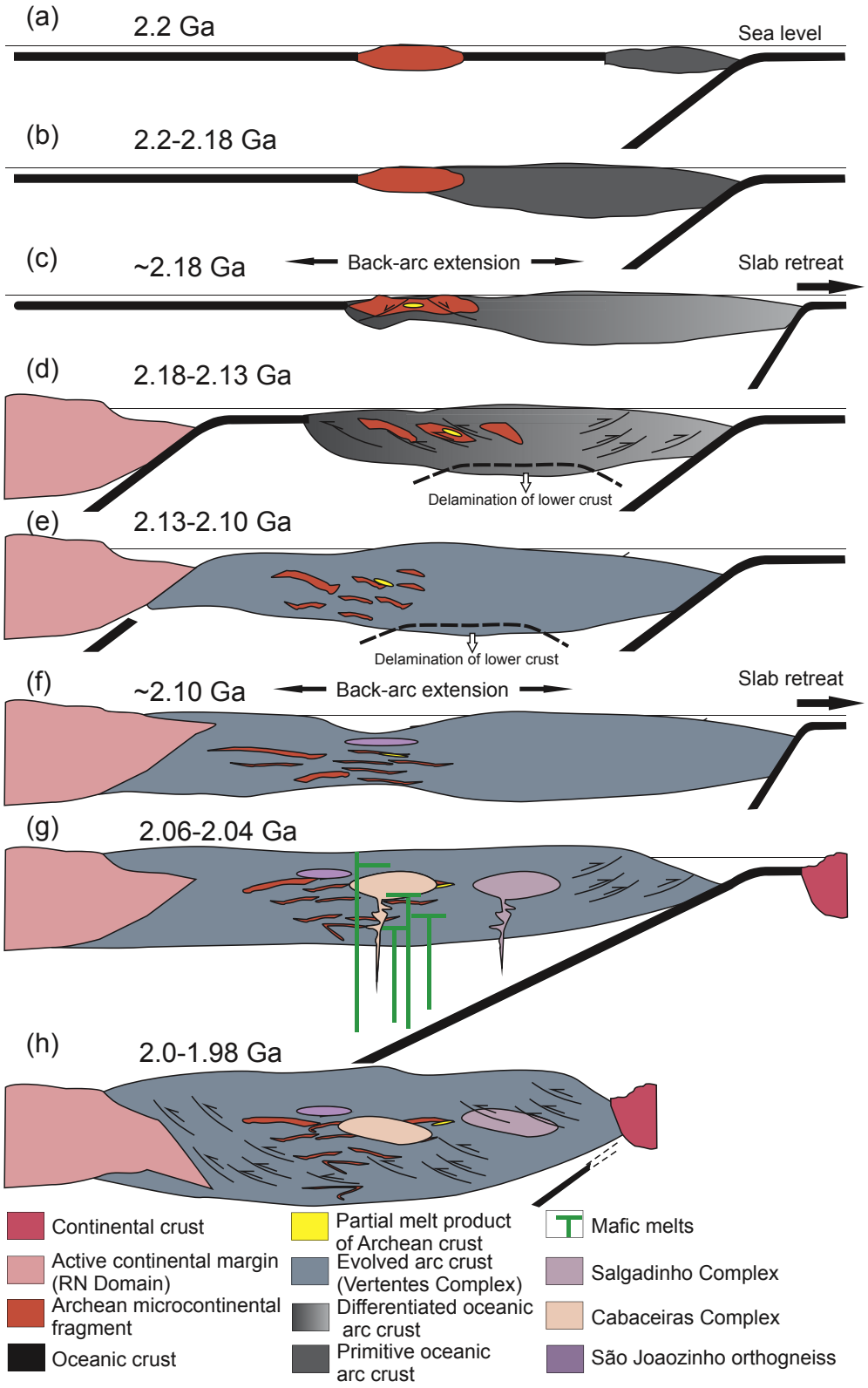

Fig. 12. Hypothetical scenario for the tectonic evolution of the study area. (a) Incipient oceanic arc inception. (b) Growing oceanic arc with microcontinental fragment in a back-arc setting. (c) Back-arc extension leading to partial melting. (d) Approach of the growing and differentiating oceanic arc to a continental active margin. (e) Main period of arc growth and differentiation, with evolution towards a more continental composition; cessation of magmatic activity in the Rio Grande do Norte Domain suggests accretion of the arc to the continental active margin sometime earlier. (f) Extension resulting from slab retreat induces partial melting, generating the protholith of the São Joaozinho orthogneiss. (g) Melts generated in the mantle wedge intrude and interact with the evolved arc crust and preexistent older continental fragments. (h) Continental collision induces regional metamorphism and syncollisional magmatism. See text for discussion.

metamorphic imprint observed on zircons of the Vertentes Complex (Fig. 5b).

The absence of rocks with ages between 2.04 and 2.01 Ga in the study area could have been consequence of continental collision (Fig. 12g), which halted subduction-related magmatism. As a result of thickening-related heat production, by 2.0–1.98 Ga, regional temperatures had increased enough to allow crustal melting, syn-collisional magmatism and metamorphism. These events were responsible for intrusion of the protolith of the felsic gneiss and for the metamorphic imprint observed in zircons of the Vertentes Complex and the orthoamphibolite.

6. Conclusion

The results of this study in conjunction with previous ones show that both crustal growth and recycling of older continental materials occurred in the eastern Borborema Province. A main period of crustal growth, represented by intrusion of calc-alkaline magmas of intermediate composition, is documented between 2.13 and 2.10 Ga. It was followed by intrusion of more evolved magmas containing variable contributions of older crustal sources at c. 2.06 Ga. Basalts (now orthoamphibolites) with island arc-related geochemistry indicate persistence of subduction zone magmatism until c. 2.04 Ga. Accordingly, a metamorphic event dated at c. 2.06–2.04 Ga is probably related with attainment of high temperature conditions at the deep levels of a thickened arc crust. In contrast, intrusion of felsic magmas coeval with regional metamorphism at 2.0–1.98 Ga probably records crustal thickening associated with continental collision.

Acknowledgments

SPN acknowledges support from the Brazilian agencies *Conselho Nacional de Desenvolvimento Científico e Tecnológico* (CNPq; grant 472582/2011-9) and *Fundação de Amparo à Ciência e Tecnologia do Estado de Pernambuco* (FACEPE; grant APQ-0479-1.07/06), and Dr. Cláudio Lamarão for providing access to the facilities of the *Universidade Federal do Pará*, where cathotoluminescence images of analyzed zircon crystals of samples SU-541, SU-49 and SU-515 were done. GAL and RGB acknowledge total support from Geological Survey of Brazil (CPRM), especially in fieldwork campaigns. The authors also thank constructive comments by two anonymous reviewers that helped to improve a previous version of the paper.

References

Dall gnoll, R., Oliveira, D.C., 2007. Oxidized, magnetite-series, rapakivi-type granites of Carajaα s, Brazil: Implications for classification and petrogenesis of A-type granites. Lithos 93, 215–233.
Almeida, F.F.M., Hasui, Y., Brito Neves, B.B., Fuck, R.A., 1981. Brazilian structural provinces: an introduction. Earth Sci. Rev. 17, 1–21.
Almeida, C.N., Guimarães, I.P., Da Silva Filho, A.F., 2002. A-type post-collisional granites in the Borborema province – NE Brazil: the Queimadas pluton. Gondwana Res. 5, 667–681.
Araújo, C.E.G., Cordani, U.G., Basei, M.A.S., Castro, N.A., Sato, K., Sproesser, W.M., 2012. U-Pb detrital zircon provenance of metasedimentary rocks from the Ceará Central and Médio Coreaú Domains, Borborema Province, NE-Brazil: tectonic implications for a long-lived Neoproterozoic active continental margin. Precambrian Res. 206-207, 36–51.
Archanjo, C.J., Hollanda, M.H.B.M., Rodrigues, S.W.O., Brito Neves, B.B., Armstrong, R., 2008. Fabrics of pre- and syntectonic granite plutons and chronology of shear zones in the Eastern Borborema Province, NE Brazil. J. Struct. Geol. 30, 310–326.
Arculus, R.J., 1994. Aspects of magma genesis in arcs. Lithos 33, 189–208.
Arthaud, M.H., Caby, R., Fuck, R.A., Dantas, E.L., Parente, C.V., 2008. Special Publications. Geology of the Northern Borborema Province, NE Brazil and its Correlation with Nigeria, NW Africa, vol. 294. Geological Society, London, pp. 49–67.
Barbarin, B., 1999. A review of the relationships between granitoid types, their origins and their geodynamic environments. Lithos 46, 605–626.
Bertrand, J.M.L., Lasserre, M., 1976. Pan-African and pre-Pan-African history of the Hoggar (Algerian Sahara) in the light of new geochronological data from the Aleksod area. Precambrian Res. 3, 343–362.
Bonin, B., 2007. A-type granites and related rocks: evolution of a concept, problems and prospects. Lithos 97, 1–29.
Boynton, W.V., 1984. Geochemistry of the rare earth elements: meteorite studies. In: Henderson, P. (Ed.), Rare Earth Element Geochemistry. Elsevier, Amsterdam, pp. 63–114.
Brasilino, R.G., Miranda, A.W.A., Marinho, M.S., 2012. Programa Geologia do Brasil. Carta Geológica – Escala 1:100 000: Folha SB.24-Z-D-VI. CPRM – Serviço Geológico do Brasil, Santa Cruz do Capibaribe.
Brito Neves, B.B., Campos Neto, M.C., Van Schmus, W.R., Santos, E.J., 2001a. O Sistema Pajeú-Paraíba e o Maciço São José do Campestre no leste da Borborema. Rev. Bras. Geociências 31, 173–184.
Brito Neves, B.B., Campos Neto, M.C., Van Schmus, W.R., Fernandes, T.M.G., Souza, S.L., 2001b. O terreno Alto Moxotó no leste da Paraíba (Maciço Caldas Brandão). Rev. Bras. Geociências 31, 185–194.
Brito Neves, B.B., Sprösser, W.M., Petronilho, L.A., Souza, S.L., 2013. Contribuição à Geologia e à Geocronologia do Terreno Rio Capibaribe (TRC, Província Borborema). In: Geologia USP, Série Científica, vol. 13, pp. 97–122.
Brown, G.C., 1977. Mantle origin of Cordilleran granites. Nature 265, 21–24.
Bruguier, O., Dada, S., Lancelot, J.R., 1994. Early Archean component (>3.5 Ga) within a 3.05 Ga orthogneiss from northern Nigeria: U-Pb zircon evidence. Earth Planet. Sci. Lett. 125, 89–103.
Buhn, B., Pimentel, M.M., Matteini, M., Dantas, E.L., 2009. High spatial resolution analysis of Pb and U isotopes for geochronology by laser ablation multi-collector inductively coupled plasma mass spectrometry (LA-MC-ICP-MS). An. Acad. Bras. Ciênc. 81, 1–16.
Cawood, P.A., Hawkesworth, C.J., Dhuime, B., et al., 2013. The continental record and the generation of continental crust. Geol. Soc. Am. Bull. 125, 14–32.
Cordani, U.G., Sato, K., 1999. Crustal evolution of the South American Platform, based on Nd isotopic systematics on granitoid rocks. Episodes 23 (3), 167–173.
Cox, K.G., Bell, J.D., Pankhurst, R.J., 1979. The Interpretation of Igneous Rocks. Allen & Unwin, London.
Da Silva Filho, A.F., Guimarães, I.P., Van Schmus, W.R., 2002. Crustal evolution of the Pernambuco-Alagoas complex, Borborema Province, NE Brazil: Nd isotopic data from Neoproterozoic granitoids. Gondwana Res. 5, 409–422.
Dada, S., 2008. Special Publications. Proterozoic Evolution of the Nigeria–Borborema Province, vol. 294. Geological Society, London, pp. 121–136.
Dall'Agnol, R., Scaillet, B., Pichavant, M., 1999. An experimental study of a Lower Proterozoic A-type granite from the eastern Amazonian craton. J. Petrol. 40, 1673–1698.
Dantas, E.L., 1997. Geocronologia U-Pb e Sm-Nd de Terrenos Arqueanos e Paleoproterozóicos do Maciço Caldas Brandão, NE do Brasil. Tese de Doutorado. UNESP, p. 208.
Dantas, E.L., Van Schmus, W.R., Hackspacher, P.C., Fetter, A., Brito Neves, B.B., Cordani, U.G., Nutman, A.P., Williams, I.S., 2004. The 3.4-3.5 Ga Sao José do Campestre massif, NE Brazil: remnants of the oldest crust in South America. Precambrian Res. 130, 113–137.
Defant, M.J., Richerson, P.M., de Boer, J.Z., Stewart, R.H., Maury, R.C., Bellon, H., Drummond, M.S., Feigenson, M.D., Jackson, T.E., 1991. Dacite genesis via both slab melting and differentiation: petrogenesis of La YeguadaVolcanic Complex, Panama. J. Petrol. 32, 1101–1142.
DePaolo, D.J., 1981. Trace element and isotopic effects of combined wall rock assimilation and fractional crystallization. Earth Planet. Sci. Lett. 53, 189–202.
Dhuime, B., Hawkesworth, C.J., Cawood, P.A., Storey, C.D., 2012. A change in the geodynamics of continental growth 3 billion years ago. Science 335, 1334–1336.
Eby, G.N., 1992. Chemical subdivision of the A-type granitoids: petrogenetic and tectonic implications. Geology 20, 641–644.
Ferré, E., Déléris, J., Bouchez, J.-L., Lar, A.U., Peucat, J.-J., 1996. The Pan-African reactivation of Eburnean and Archean provinces in Nigeria: structural and isotopic data. J. Geol. Soc. Lond. 153, 719–728.
Ferreira, V.P., Sial, A.N., Jardim de Sá, E.F., 1998. Geochemical and isotopic signatures of Proterozoic granitoids in terranes of the Borborema structural province, northeastern Brazil. J. South Am. Earth Sci. 11, 439–455.
Fetter, A.H., Van Schmus, W.R., Santos, T.J.S., Nogueira Neto, J.A., Arthaud, M.H., 2000. U-Pb and Sm-Nd geochronological constraints on the crustal evolution of basement architecture of Ceará state, NW Borborema province, NE Brazil: implications for the existence of the Paleoproterozoic supercontinent 'Atlantica'. Rev. Bras. Geociências 30, 102–106.
Frost, B.R., Barnes, C., Collins, W., Arculus, R., Ellis, D., Frost, C., 2001. A chemical classification for granitic rocks. J. Petrol. 42, 2033–2048.
Gióia, S.M.C.L., Pimentel, M.M., 2000. The Sm-Nd isotopic method in the geochronology laboratory of the University of Brasília. An. Acad. Bras. Ciências 72, 220–245.
Guimarães, I.P., Da Silva Filho, A.F., Almeida, C.N., Van Schmus, W.R., Araújo, J.M.M., Melo, S.C., Melo, E.B., 2004. Brasiliano (Pan-African) granite magmatism in the Pajeú-Paraíba belt, Northeast Brazil: an isotopic and geochronological approach. Precambrian Res. 135, 23–53.
Guimarães, I.P., Van Schmus, W.R., Brito Neves, Bittar, S.M.B., Da Silva Filho, A.F., Armstrong, R., 2012. U–Pb zircon ages of orthogneisses and supracrustal rocks of the Cariris Velhos belt: onset of Neoproterozoic rifting in the Borborema Province, NE Brazil. Precambrian Res. 192–195, 52–77.
Hackspacher, P.C., Van Schmus, W.R., Dantas, E.L., 1990. Um embasamento Transamazônico na Província Borborema. In: Nordeste, S.N. (Ed.), 36 Congr. Bras. Geol., Natal, pp. 2683–2696.

Hargrove, U.S., Stern, R.J., Kimura, J.I., Manton, W.I., Johnson, P.R., 2006. How juvenile is the Arabian–Nubian Shield? Evidence from Nd isotopes and pre-Neoproterozoic inherited zircon in the Bi'r Umq suture zone, Saudi Arabia. Earth Planet. Sci. Lett. 252, 308–326.
Hawkesworth, C., Dhuime, B., Pietranik, A., Cawood, P., Kemp, T., Storey, C., 2010. The generation and evolution of the continental crust. J. Geol. Soc. Lond. 167, 229–248.
Hollanda, M.H.B.M., Pimentel, M.M., Jardim de Sá, E.F., 2003. Paleoproterozoic subduction-related metasomatic signatures in the lithospheric mantle beneath NE Brazil: inferences from trace element and Sr-Nd-Pb isotopic compositions of Neoproterozoic high-K igneous rocks. J. South Am. Earth Sci. 15, 885–900.
Hollanda, M.H.B.M., Archanjo, C.J., Souza, L.C., Dunyi, L., Armstrong, R.A., 2011. Long-lived Paleoproterozoic granitic magmatism in the Seridó-Jaguaribe domain, Borborema Province–NE Brazil. J. South Am. Earth Sci. 32, 287–300.
Irvine, T.N., Baragar, W.R., 1971. A guide to the chemical classification of the common volcanic rocks. Can. J. Earth Sci. 8, 523–548.
Jagoutz, O., Behn, M.D., 2013. Foundering of lower island-arc crust as an explanation for the origin of the continental Moho. Nature 504, 131–134.
Jagoutz, O., Schmidt, M.W., 2013. The composition of the foundered complement to the continental crust and are-evaluation of fluxes in arcs. Earth Planet. Sci. Lett. 371–372, 177–190.
Janoušek, V., Farrow, C.M., Erban, V., 2006. Interpretation of whole-rock geochemical data in igneous geochemistry: introducing Geochemical Data Toolkit (GCDkit). J. Petrol. 47, 1255–1259.
Jung, S., Mezger, K., Hoernes, S., 1998. Petrology and geochemistry of syn- to post-collisional metaluminous A-type granites – a major and Nd-Sr-Pb-O-isotope study from the Proterozoic Damara Belt, Namibia. Lithos 45, 147–175.
Kay, R.W., Kay, S.M., 1993. Delamination and delamination magmatism. Tectonophysics 219, 177–189.
King, P.L., White, A.J.R., Chappell, B.W., Allen, C.M., 1997. Characterization and origin of aluminous A-type granites from the Lachlan Fold Belt, southeastern Australia. J. Petrol. 38, 371–391.
Kroner, A., 1977. The Precambrian geotectonic evolution of Africa: plate accretion versus plate destruction. Precambrian Res. 4, 163–213.
Lages, G.A., Marinho, M.S., 2012. Programa Geologia do Brasil. Carta Geológica – Escala 1:100 000: Folha SB.24-Z-D-III, Boqueirão. CPRM – Serviço Geológico do Brasil.
Li, D., He, D., Shantosh, M., Tang, J., 2014. Petrogenesis of Late Paleozoic volcanics from the Zhaheba depression, East Junggar: Insights into collisional event in an accretionary orogeny of Central Asia. Lithos 184–187, 167–193.
Lister, G., Foster, M., 2009. Tectonic mode switches and the nature of orogenesis. Lithos 113, 274–291.
Ludwig 2000.
Mariano, G., Neves, S.P., Da Silva Filho, A.F., Guimarães, I.P., 2001. Diorites of the high-K calc-alkalic association: geochemistry and Sm-Nd data and implications for the evolution of the Borborema province, Northeast Brazil. Int. Geol. Rev. 43, 921–929.
Martin, H., 1986. Effect of steeper Archean geothermal gradient on geochemistry of subduction-zone magma. Geology 14, 753–756.
Martins, G., Oliveira, E.P., Lafon, J.M., 2009. The Algodões amphibolite–tonalite gneiss sequence, Borborema Province, NE Brazil: geochemical and geochronological evidence for Palaeoproterozoic accretion of oceanic plateau/back-arc basalts and adakitic plutons. Gondwana Res. 15, 71–85.
McDonough, W.F., Sun, S.S., 1995. The composition of the Earth. Chem. Geol. 120, 223–253.
Medeiros, V.C., Medeiros, W.E., Jardim de Sá, E.F., 2011. Utilização de imagens aerogamaespectrométricas, Landsat 7 ETM+ e aeromagnéticas no estudo do arcabouc.o crustal da porção central do Domínio da Zona Transversal, Província Borborema, NE do Brasil. Rev. Bras. Geofísica 29, 83–97.
Neves, S.P., 2015. Constrains from zircon geochronology on the tectonic evolution of the Borborema Province (NE Brazil): widespread Neoproterozoic intracontinental reworking of a Paleoproterozoic accretionary orogen. J. South Am. Earth Sci. 58, 150–164.
Neves, S.P., Alcantara, V.C., 2010. Geochemistry of orthogneisses and metasedimentary rocks across a proposed terrane boundary in the Central Domain of Borborema Province, NE Brazil: geodynamic implications. J. South Am. Earth Sci. 29, 498–511.
Neves, S.P., Mariano, G., 1999. Assessing the tectonic significance of a large-scale transcurrent shear zone system: the Pernambuco lineament, northeastern Brazil. J. Struct. Geol. 21, 1369–1383.
Neves, S.P., Vauchez, A., 1995. Successive mixing and mingling of magmas in a plutonic complex of Northeast Brazil. Lithos 34, 275–299.
Neves, S.P., Vauchez, A., Feraud, G., 2000. Tectono-thermal evolution, magma emplacement, and shear zone development in the Caruaru area (Borborema Province, NE Brazil). Precambrian Res. 99, 1–32.
Neves, S.P., Melo, S.C., Moura, C.A.V., Mariano, G., Silva, J.M.R., 2004. Zircon Pb-Pb geochronology of the Caruaru area, northeastern Brazil: temporal constraints on the Proterozoic evolution of Borborema Province. Int. Geol. Rev. 46, 52–63.
Neves, S.P., Silva, J.M.R., Mariano, G., 2005. Oblique lineations in orthogneisses and supracrustal rocks: vertical partitioning of strain in a hot crust (eastern Borborema Province, NE Brazil). J. Struct. Geol. 27, 1513–1527.
Neves, S.P., Bruguier, O., Vauchez, A., Bosch, D., Silva, J.M.R., Mariano, G., 2006. Timing of crust formation, deposition of supracrustal sequences, and Transamazonian and Brasiliano metamorphism in the East Pernambuco belt (Borborema Province, NE Brazil): Implications for western Gondwana assembly. Precambrian Res. 149, 197–216.
Neves, S.P., Bruguier, O., Bosch, D., Silva, J.M.R., Mariano, G., 2008. U–Pb ages of plutonic and metaplutonic rocks in southern Borborema Province (NE Brazil): timing of Brasiliano deformation and magmatism. J. South Am. Earth Sci. 25, 285–297.
Neves, S.P., Bruguier, O., Silva, J.M.R., Bosch, D., Alcantara, V.C., Lima, C.M., 2009. The age distributions of detrital zircons in metasedimentary sequences in eastern Borborema Province (NE Brazil): evidence for intracontinental sedimentation and orogenesis? Precambrian Res. 175, 187–205.
Neves, S.P., Mariano, G., Silva, J.M.R., 2010. Programa Geologia do Brasil. Carta Geológica – Escala 1:100 000: Folha SB.25-Y-C-IV, Surubim. CPRM – Serviço Geológico do Brasil.
Njiosseu, E.L.T., Nzenti, J.P., Njanko, T., Kapajika, B., Nédélec, A., 2005. New U-Pb zircon ages from Tonga (Cameroon): coexisting Eburnean-Transamazonian (2.1 Ga) and Pan-African (0.6 Ga) imprints. Comptes Rendus Geosci. 337, 551–562.
Patiño Douce, A.E., Beard, J.S., 1995. Dehydration-melting of biotite gneiss and quartz amphibolite from 3 to 15 kbar. J. Petrol. 36 (3), 707–738.
Pearce, J.A., 1982. Trace element characteristics of lavas from destructive plate boundaries. In: Thorpe, R.S. (Ed.), Andesites: Orogenic Andesites and Related Rocks. Wiley, Chichester, pp. 525–548.
Pearce, J.A., Cann, J.R., 1973. Tectonic setting of basic volcanic rocks determined using trace element analyses. Earth Planet. Sci. Lett. 19, 290–300.
Pearce, J.A., Norry, M.J., 1979. Petrogenetic implications of Ti, Zr, Y, and Nb variations in volcanic rocks. Contrib. Mineral. Petrol. 69, 33–47.
Peccerillo, R., Taylor, S.R., 1976. Geochemistry of Eocene cal-alkaline volcanic rocks from the Kastamonu area, northern Turkey. Contrib. Mineral. Petrol. 58, 63–81.
Petrelli, M., Poli, G., Perugini, D., Peccerillo, A., 2005. PetroGraph: a new software to visualize, model, and present geochemical data in igneous petrology. Geochem. Geophys. Geosyst. 6, Q07011. http://dx.doi.org/10.1029/2005GC000932.
Rodrigues, S.W.O., Brito Neves, B.B., 2008. Padrões isotópicos Sm-Nd no limite entre os terrenos Alto Pajeú e Alto Moxotó (PB). Rev. Bras. Geociências 38, 209–225.
Rodrigues, S.W.O., Medeiros, V.C., Brasilino, R.G., 2010a. U/Pb Geochonology of Salvador Orthogneiss (Paleoproterozoic unit of Transversal zone, Borborema Province) in Campina Grande sheet (SB.25-Y-C-I). In: VII South American Symposium on Isotope Geology. CD-ROM, Brasília.
Rodrigues, S.W.O., Medeiros, V.C., Brito Neves, B.B., Marinho, M.S., Gusmão, R.O., 2010b. Programa Geologia do Brasil. Carta Geológica – Escala 1:100 000: Folha SB.25-Y-C-I, Campina Grande. CPRM – Serviço Geológico do Brasil.
Rushmer, T., 1991. Partial melting of two amphibolites: contrasting experimental results under fluid-absent conditions. Contrib. Mineral. Petrol. 107, 41–59.
Sá, J.M., Bertrand, J.M., Leterrier, J., Macedo, M.H.F., 2002. Geochemistry and geochronology of pre-Brasiliano rocks from the Transversal Zone, Borborema Province, Northeast Brazil. J. South Am. Earth Sci. 14, 851–866.
Sakuyama, M., Nesbitt, R.W., 1986. Geochemistry of the Quaternary volcanic rocks of the northeast Japan arc. J. Volcanol. Geotherm. Res. 29, 413–450.
Santos, E.J., Nutman, A.P., Brito Neves, B.B., 2004. Idades SHRIMP U-Pb do Complexo Sertânia: implicações sobre a evolução tectônica da zona transversal, Província Borborema. In: Geologia USP: Série Científica, vol. 4, pp. 1–12.
Santos, T.J.S., Fetter, A.H., Hackspacher, P.C., Van Schmus, W.R., Nogueira Neto, J.A., 2008. Neoproterozoic tectonic and magmatic episodes in the NW sector of Borborema Province, NE Brazil, during assembly of Western Gondwana. J. South Am. Earth Sci. 25, 271–284.
Santos, E.J., Souza Neto, J.A., Carmona, L.C.M., Armstrong, R., Santos, L.C.M.L., Mendes, L.U.S., 2013. The metacarbonate rocks of Itatuba (Paraíba): a record of sedimentary recycling in a Paleoproterozoic collision zone of the Borborema province, NE Brazil. Precambrian Res. 224, 454–471.
Souza, Z.S., Martin, H., Peucat, J.J., Jardim de Sá, E.F., Macedo, M.H.F., 2007. Calc-alkaline magmatism at the Archean-Proterozoic Transition: the Caicó Complex basement (NE Brazil). J. Petrol. 48, 2149–2185.
Torsvik et al, 2013. A Precambrian microcontinent in the Indian Ocean. Nat. Geosci. 6, 223–227.
Toteu, S.F., Van Schmus, W.R., Penaye, J., Michard, A., 2001. New U–Pb and Sm–Nd data from north-central Cameroon and its bearing on the pre-Pan African history of central Africa. Precambrian Res. 108, 45–73.
Van Schmus, W.R., Brito Neves, B.B., Hackspacher, P., Babinski, M., 1995. U/Pb and Sm/Nd geochronologic studies of the eastern Borborema Province, northeastern Brazil: initial conclusions. J. South Am. Earth Sci. 8, 267–288.
Van Schmus, W.R., Brito Neves, B.B., Williams, I.S., Hackspacher, P., Fetter, A.H., Dantas, E.L., Babinski, M., 2003. The Seridó Group of NE Brazil, a late Neoproterozoic pre- to syn-collisional basin in West Gondwana: insights from SHRIMP U-Pb detrital zircon ages and Sm-Nd crustal residence (TDM) ages. Precambrian Res. 127, 287–327.
Van Schmus, W.R., Oliveira, E.P., Da Silva Filho, A., Toteu, S.F., Penaye, J., Guimarães, I.P., 2008. Special Publications. Proterozoic Links between the Borborema Province, NE Brazil, and the Central African Fold Belt, vol. 294. Geological Society, London, pp. 69–99.
Van Schmus, W.R., Kozuch, M., Brito Neves, B.B., 2011. Precambrian history of the Zona Transversal of the Borborema Province, NE Brazil: Insights from Sm-Nd and U-Pb geochronology. J. South Am. Earth Sci. 31, 227–252.
Whalen, J.B., Currie, K.L., Chappell, B.W., 1987. A-type granites: geochemical characteristics, discrimination and petrogenesis. Contrib. Mineral. Petrol. 95, 407–419.
Yuan, C., Sun, M., Wilde, S., X iao, W., Xu, Y., Long, X., Zhao, G., 2010. Post-collisional plutons in the Balikun area, East Chinese Tianshan: evolving magmatism in response to extension and slab break-off. Lithos 119, 269–288.